

FEBRUARY 2017

M.Sc. in Civil Engineering

ARKAN HAMZA IBRAHIM

**UNIVERSITY OF GAZIANTEP
GRADUATE SCHOOL OF
NATURAL & APPLIED SCIENCES**

**MODELING SCOURING AROUND BRIDGE PIERS WITH
DIFFERENT GEOMETRIES**



**M. Sc. THESIS
IN
CIVIL ENGINEERING**

**BY
ARKAN HAMZA IBRAHIM
FEBRUARY 2017**

Modeling Scouring Around Bridge Piers with Different Geometries



M.Sc. Thesis
in
Civil Engineering
University of Gaziantep

Supervisor

Prof. Dr. Mustafa GÜNAL

by

Arkan Hamza IBRAHIM

February 2017



© 2017 [Arkan Hamza IBRAHIM]


REPUBLIC OF TURKEY
UNIVERSITY OF GAZIANTEP
GRADUATE SCHOOL OF NATURAL & APPLIED SCIENCES
CIVIL ENGINEERING DEPARTMENT

Name of the thesis: Modeling Scouring Around Bridge Piers with Different Geometries.

Name of the student: ARKAN HAMZA IBRAHIM

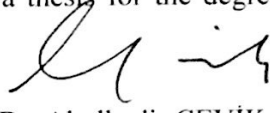
Exam date:14.02.2017

Approval of the Graduate School of Natural and Applied Sciences


Prof. Dr. A. Necmeddin YAZICI


Director

I certify that this thesis satisfies all the requirements as a thesis for the degree of Master of Science.


Prof. Dr. Abulkadir ÇEVİK

Head of Department

This is to certify that we have read this thesis and that in our consensus opinion it is fully adequate, in scope and quality, as a thesis for the degree of Master of Science.


Prof. Dr. Mustafa GÜNAL
Supervisor

Examining Committee Members

Prof. Dr. Mustafa GÜNAL

Doç. Dr. Aytaç GÜVEN

Dr. Ali AYTEK

Signature



I hereby declare that all information in this document has been obtained and presented in accordance with academic rules and ethical conduct. I also declare that, as required by these rules and conduct, I have fully cited and referenced all material and results that are not original to this work.

Arkan Hamza IBRAHIM

ABSTRACT

MODELING SCOURING AROUND BRIDGE PIERS WITH DIFFERENT GEOMETRIES

SIBRAHIM, Arkan Hamza

**IBRAHIM, Arkan Hamza
M.Sc. in Civil Engineering**

Supervisor: Prof. Dr. Mustafa GÜNAL

February 2017

81 pages

Scouring around bridge pier considered as one of the main reasons of bridge failure. Failure of the bridge structure is a catastrophic phenomenon. Studying the causes of scouring will give an idea about the solution probabilities, the shape and geometry of bridge piers has a great influence on the local scour. A literature review showed that there is still a lack of experimental and numerical investigation on the influence of the non-uniform pier geometry. Flow-3D was used for simulating of three-dimensional model to study local scouring around three different models of bridge piers based on an experimental study from literature which is performed to study the probability of reducing local scouring around a three different bridge pier models, one circular model and two non-uniform pier shapes with different orientations of bridge piers named as “upstream-facing round nosed pier (US-FRNP) (10-4)cm” and “downstream-facing round nosed pier (DS-FRNP) (4-10)cm” according to flow direction in a fixed flatbed and scoured bed condition. The results showed a good agreement between the experimental and numerical models and result from comparisons from both studies reveal that “downstream facing round-nosed bridge pier (DS-FRNP)” is an efficient countermeasure to lessen both scour depth and volume.

Key Words: Bridge pier, Sediment Scour, Scour Reduction, Flow-3D, Bed-load erosion.

ÖZET

FARKLI GEOMETRİDEKİ KÖPRÜ AYAKLARI ETRAFINDA OLUŞAN YEREL OYULMANIN MODELLENMESİ

İBRAHİM, Arkan Hamza

Yüksek Lisans Tezi, İnşaat Mühendisliği Bölümü

Tez Yöneticisi: Prof. Dr. Mustafa GÜNAL

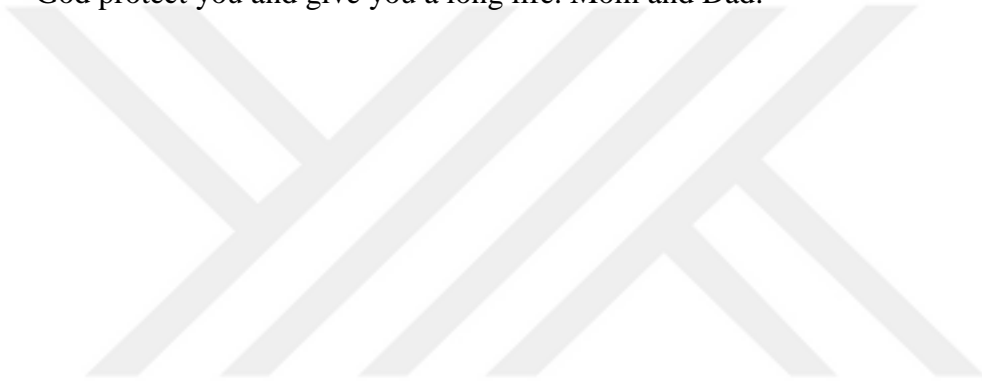
Şubat 2017

81 sayfa

Köprü ayakları etrafında oluşan oyulma, köprülerin zarar görmesinin ana nedenlerinden biridir. Köprünün yıkılması felaket bir olaydır. Oyulma nedenlerini incelemek, yerel oyulma üzerinde büyük bir etkiye sahip olan köprü ayak şekli ve geometrisi ve çözüm olasılıkları hakkında bir fikir verecektir. Bu konuda yapılan çalışmalar düzgün olmayan köprü ayak şekillerinin geometrisi hakkında yeterli deneysel ve sayısal çalışma olmadığını göstermektedir. Flow-3D, üç farklı köprü ayak modelinin etrafında oluşan yerel oyulmayı azaltma olasılığını incelemek üzere gerçekleştirilen deneysel bir literatür araştırmasına dayanan, üç köprü ayağı çevresinde oluşan yerel oyulmayı incelemek için kullanıldı. Dairesel model ve "membaya bakan yuvarlak burunlu köprü ayağı (US-FRNP) (10-4) cm" ve "mansaba bakan yuvarlak burunlu köprü ayağı (DS-FRNP) (4-10) cm" köprü ayağı modeli sabit ve hareketli taban koşulunda sayısal modelleme yapılmıştır. Sonuçlar, deneysel ve sayısal modeller arasında mükemmel bir anlaşma olduğunu ve her iki çalışmanın karşılaştırmalarının sonucu olarak, "mansaba bakan yuvarlak burunlu köprü ayağı (DS-FRNP)" modeli oyulma derinliğini ve hacmini azaltmak için etkili bir karşı önlem olduğunu ortaya koymaktadır.

Anahtar Kelimeler: Köprü ayağı, Yerel oyulma, Oyulma, Flow-3D.

Without you, this could more than difficult I am very lucky that I have you, May
God protect you and give you a long life. Mom and Dad.



ACKNOWLEDGEMENTS

The author wishes to express his deepest gratitude to his supervisor Prof. Dr. Mustafa GÜNAL for his guidance, advice, criticism, encouragements and insight throughout the research.

Similarly, I want to express my appreciation to all the teachers at Hydraulic division for their support and encouragement during the study.

Finally, I am so thankful to my lovely wife for her help and care through different stages of the study.

TABLE OF CONTENTS

	Page
ABSTRACT	vi
ÖZET	vii
ACKNOWLEDGEMENTS	viii
TABLE OF CONTENTS	ix
LIST OF TABLES	xii
LIST OF FIGURES	xiii
LIST OF SYMBOLS/ABREVIATIONS	xv
CHAPTER 1	1
INTRODUCTION	1
1.1 General	1
1.2 General Scouring Terminology	5
1.3 Study Objective	7
1.4 Outline of Thesis	7
CHAPTER 2	9
LITERATURE REVIEW	9
2.1 Introduction	9
2.2 Scour types	9

2.2.1 General scour	9
2.2.2 Localized scour	10
2.2.3 Contraction scour	10
2.2.4 Live-bed scour	11
2.3 Sediment transport around bridge piers.....	11
2.3.1 Down-flow at the pier face	11
2.3.2 Horseshoe vortex	12
2.3.3 Bow waves	12
2.3.4 Wake vortex	12
2.4 Effect of the shape of the pier	14
2.5 CFD modeling	17
2.6 Studies about bridge pier scour in general	21
2.7 Initial motion of sediment particles	23
CHAPTER 3	28
MODEL SETUP	28
3.1 Introduction	28
3.2 Experimental Procedure	28
3.3 The Numerical Modelling	31
3.4 Sediment Scour parameters and modelling	33
3.4.1 Meshing setup	34
3.4.2 Specifying Boundary Conditions	35

3.4.3 Physics and Numerical Options	36
CHAPTER 4	37
RESULT AND DISCUSSION	39
4.1 Introduction	39
4.2. Comparison of simulated and experimental results	39
4.3 Flow field and velocity magnitude	43
4.4 Scour development versus time.....	45
4.5 Scour hole versus velocity profiles.....	50
4.6 Correlation of scour depth versus the Froude number	51
4.6 Velocity vector distribution and their effect.....	53
4.7 Scour depth versus turbulent intensity	53
CHAPTER 5	53
CONCLUSIONS AND RECOMMENDATIONS	56
5.1 CONCLUSION	56
5.2 Recommendation.....	58
REFERENCES	60
APPENDICES	68
APPENDIX A	69
APPENDIX D	80

LIST OF TABLES

	Page
Table 2.1 Numerical and measured depth of scour comparison at Pennsylvania bridge.....	21
Table 3.1 The Test conditions.....	33
Table 4.1 Maximum Depth of scour for physical & numerical models.....	40

LIST OF FIGURES

	Page
Figure 1.1 Types of Scour at bridge channels.....	5
Figure 2.1 Flow pattern around circular pier	13
Figure 2.2 Different pier shapes tested for scour reduction.	15
Figure 2.3 Effect of angle of attack vs the depth of scour for different shapes..	16
Figure 2.4 Shape coefficient (ratio of depth of scour of a specific pier shape according to a rectangular pier).....	17
Figure 2.5 Time-based variation of the local scour around the side-by-side arrangement compared to triangular arrangement of the piers.....	19
Figure 2.6 The main forces acting on a sediment particle and their direction.	24
Figure 3.1 Schematic layout of the flume	29
Figure 3.2 Shape and dimensions of tested bridge piers	29
Figure 3.3 Grain size distributions.....	30
Figure 3.5 Computational domain and mesh setup around the Bridge pier	35
Figure 3.6 Boundary conditions.....	36
Figure 4.1 Maximum Scour hole development for experimental and CFD model of each tested pier (58 l/s).	41

Figure 4.2 Crosswise scour holes of three different bridge piers a-Experimental models b-CFD models (b-1. circular b-2. UFRNP 10-4, b-3. DFRNP 4-10).....	42
Figure 4.3 Flow around the circular pier at 15 min.....	44
Figure 4.4 3D Plots of scour holes around the all the models at different time.	49
Figure 4.5 Depth of scour (in negative value) and height of sediment deposition (in positive value) at different time.	50
Figure 4.6 Scour hole versus velocity profiles.....	51
Figure 4.7 Correlation of Froude number versus the scour depth.....	52
Figure 4.8 Velocity vectors at vertical plane a circular pie, b upstream facing round-nosed pier and c downstream facing round-nosed pier	54
Figure 4.9 Scour depth versus turbulent intensity.....	55

LIST OF SYMBOLS/ABBREVIATIONS

FL	Lift or buoyancy force
FW	Downward force from the submerged weight
FR	Resistance force
FD	Is the drag force.
$\tau c *$	Critical Shields value
Re	Reynolds number
Re^*	Shear Reynolds number.
τbc	Critical bed shear stress for start of motion
$U*c$	Critical shear velocity
ρs	Density of sediment and correspondingly (kg/m^3)
ρ	water density (kg/m^3)
D	Diameter of the sediment particle
g	Gravity of the sediment particle (m/s^2)
U	Velocity of flow (m/s)
d_{50}	Median particle diameter of the sediments (mm)
U^*	Shear velocity
F_R	Froude number (U/\sqrt{gH})
F_O	Dens metric Froude number
US-FRNP	Upstream-facing round nosed pier (10-4) cm.
DS-FRNP	Downstream-facing round nosed pier (4-10) cm.
TKE	Turbulent kinetic energy
RMS	Root mean square

CFD	Computational Fluid Dynamics
b	Pier width (m)
u	Flow velocity (m/s)
h	Flow depth (m)



CHAPTER 1

INTRODUCTION

1.1 General

Formation of scours holes that undermine bridge pier and abutment foundations in the time of great flood events are one of the chief causes for the bridge failure (Tulimilli et al., 2003) which take place as erosion. As the United Nations Environment Program states, erosion is one of the most potentially hazardous physical phenomena occurred in semi-arid regions (UNEP, 2000). Erosion occurs when flows exert shear stresses on solid boundaries over a certain threshold, which depends on soil type, granulomere, temperature, etc. (Moody et al., 2005). Studying erosion in the river bed considered as an important part of designing transportation systems and bridges piers size and geometry. Sudden increases in shear stress can occur due to changes of flow regime (Wu and Rajratnam, 1996) or geometry (Pitt et al., 2007). It has been estimated that processes involving river hydraulics lead to bridges failure about 60% like pier scour (Melville and Coleman, 2000). Nearly about one thousand bridges structures in the United States of America have collapsed during the last 4 decades leading to a great economic loss in Georgia, the over-all economic damage from tropical storm Alberto in 1994 estimated nearly as \$130 million. About 100 bridges needed to be replaced and fixed because of flooding (Richardson and Davis, 2001). Also in Turkey, There have been many floods lead to bridge failures during last decades, some of these floods occurred in Trabzon (1990), Malatya (1991), Bartın (1998), Hatay (2001), and Mersin (2001) (Yanmaz, 2002).

Even though considerable laboratory investigations have been done on scour at certain sorts of structures, for example bridge piers, yet there are substantial gaps in data and over-all understanding. During high flows, it's difficult to make field measurements at structures which tends to hide the latent importance of the problem since scouring holes may refill when the flood peak is gone. The resulting absence of consistent field data has made it hard to confirm estimates of latent scour depths gained from small-scale laboratory examinations. It is possible that various laboratory examinations have over-simplified the complex nature of scouring phenomena, but still, the best practice is experiment study which can be used along with numerical models and more real life case can be simulated after model validation.

In 1914 Gilbert proposed the first equation for estimating sediment transport. Later then, various equations for sediment transport have been proposed for either single or multi-grain sediment size in a steady state and uniform flow in open channel. Those equations used in different sediment transport modes like those which aimed at total sediment load that does not separate bed load and suspended load, also while others only for suspended load or bed load amid them, Engineers use equations of total load most commonly.

Physical models are widely used for designing large hydraulic structures before the presence of computer technology, for instance designing dams, Canals. By the time of technology development in computers, specifically personal computers at home or work place, computational models now are becoming a dependable and economic tool for engineering design purposes. An authorized and confirmed computational model give chance to be reused for investigating many design options. At the present time computational modeling investigations is vital for hydraulic engineering design

purposes, watershed calculations, and river studies. CFD models which now being used for hydraulic engineering are initially advanced for mechanical engineering and are improved version of it. Numerical models can be used for simulation of a different of flow field modeling, such as flow above and downstream of hydraulic structures around bridge piers structures, dikes, at river meandering bends and river convergence. Even though numerical models have a great effect on engineering designs economically, few CFD models are accurate for turbulent flow field around bridge pier by reason of the restrictions of boundary conditions, turbulence closures, and/or numerical techniques. It is a necessary to check the accurateness of the numerical model's hydrodynamic simulations through the comparison of the numerical model and the laboratory experimental results.

Determining the mean and turbulence flow field around the bridge pier structures and their effect on the stability of the bridge structure in engineering design often done by using three- dimensional models. However, currently, there is no worldwide turbulent model available that is accurate for different turbulent flow cases in open channels. Some turbulent closures are more suitable than other turbulent models in specific flow field depending on the kind of turbulence. Turbulent closures, like eddy viscosity and mixing-length models, considered as more applicable to engineering field practice where fewer detailed data of turbulent variations and Reynolds stresses is needed. Simulations with further detailed turbulent flow field are required to study local scour development as a result of turbulence. Equations of turbulent models start with the standard $k-\varepsilon$ model which solves two transport equations for turbulent kinetic energy in addition to its dissipation rate for eddy viscosity calculation. In addition to the standard $k-\varepsilon$ model, many modified $k-\varepsilon$ models, for example renormalized and realizable $k-\varepsilon$ models are similarly existing for complex flow field

around bridge piers. Yet, the applicability of each turbulence closure models to turbulent flow field near bridge piers stays unfamiliar. That's why it shows the need of finding the proper turbulence model for simulating turbulence flow field around bridge piers.

The sediment model in HEC-RAS 4.1 that recently developed composed of total of five load equations and two-bed load equations (HEC 2010). Even though all of the formulas were verified also checked through using sequence of experimental and field studies, calculations using these formulas mostly order-of-magnitude change for the similar hydraulic state. Unreliable outcomes using these sediment transport methods reveals that the predicting the sediment transport phenomenon is yet not complete, particularly how immediate flow turbulence entrain and transport sediment particles, also in what way bed shear stresses enhance sediment transport.

There are no equations available in sediment transport that has been approved universally to calculate the rate of total sediment transport. Hence, estimating the total sediment load in open channels remain a challenge to hydraulic engineers and needs a worldwide formula that unites the present equations and gives precise predictions of current extents.

Bridge scour nearly include all forms of waterway erosion that take place within and close to the bridge waterways which are generally denoted as

- General scouring and,
- Local scouring

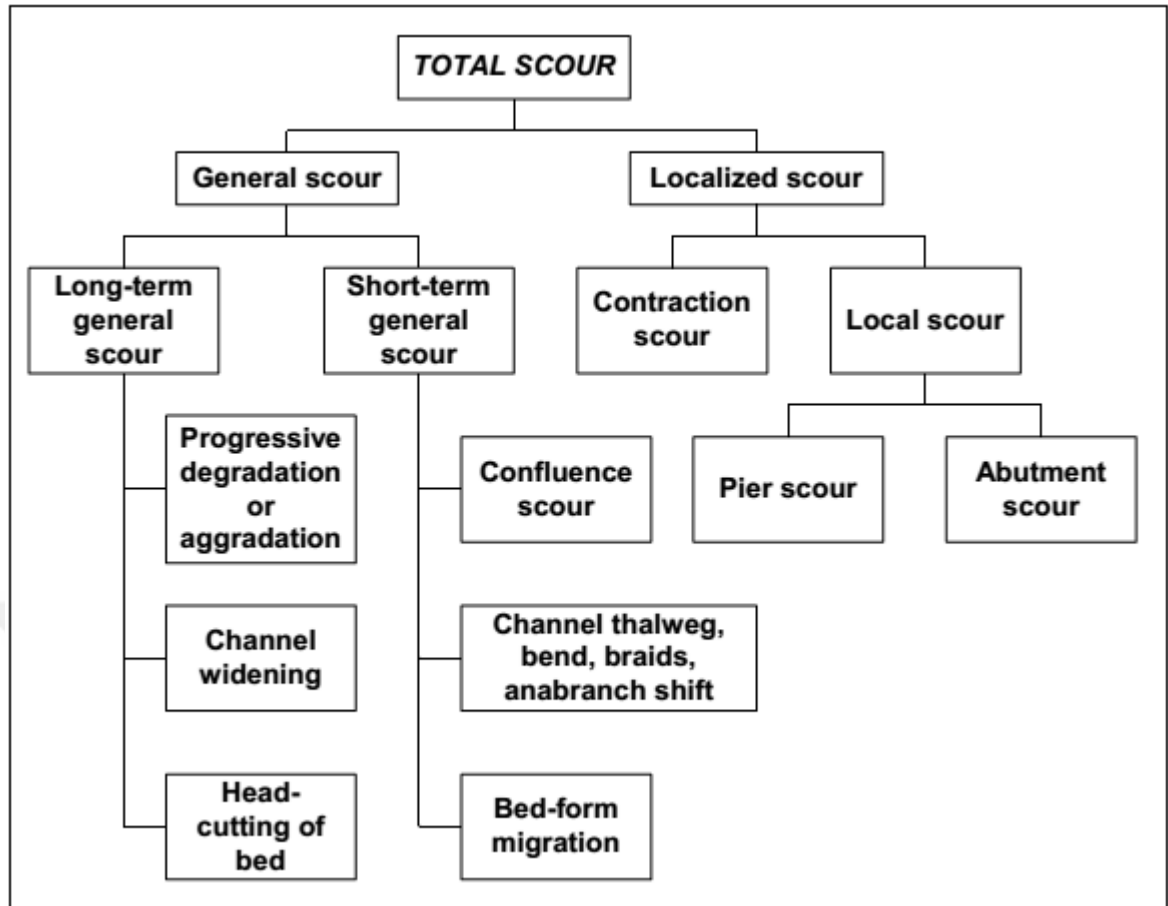


Figure 1.1 Types of Scour at bridge channels (Robert et al., 2006)

1.2 General Scouring Terminology

The types of scour that take place in open channel flow are usually indicate to us general scour and local scour, that includes both of contraction scouring and local scouring. Types of scour categorized in Figure 1-1 are described as:

- Total scour includes both general and localized scour, and it's the over-all depth of scour at a certain bridge foundation.
- General scour consist of long-term general scour and short-term general scours, and it's the scour that takes place regardless of the presence of the bridge structure.
- Long-term scour comprises of progressive degradation or aggradation and bank lateral erosion as a result of channel widening or meander movement. This type of

scour that needs a timescale up to several years or more to take place with and progressive degradation nearly is permanent depressing of the waterway bed around a bridge location by reason of ordinary variations in the watershed. On the other hand, the overall downstream rising of the riverbed soil at the bridge site for example, as a result of dam building called progressive aggradation.

- Short-term general scour is scouring which occurs in the time of a single or several floods following each other, it contains scour on a convergence, a move in river thalweg moves in bends at channel sides, also scour appear from bed-form (dune or bar) relocation.

- Local scour is scouring which is directly related to the presence of the bridge piers and abutments, that contains scouring due to flow contraction in addition to the local flow field occurs at a bridge pier structure.

- Contraction scour is that type of scour that happens since the flow is constricted by means of the presence of bridge structures.

- Localized scour produced by the flow field shaped at a bridge and its approaches. That is noted as pier scouring and abutment scouring.

- Jet scour takes place after construction of a road way drainage into the river lengthways the edge of an abutment of the drainage structure.

On any bridge constructed in a river, all of the above-mentioned scouring types can happen instantaneously. For design purposes, it is required to ensure that the overall scour comprises a proper grouping of the scour categories. A humble diagram in figure 1.2 shows the scour forms frequently detected within the bridge maiden. Depths of scour typically are supreme adjacent to bridge abutments and piers, as the flow fields produced through all those mechanisms of a bridge.

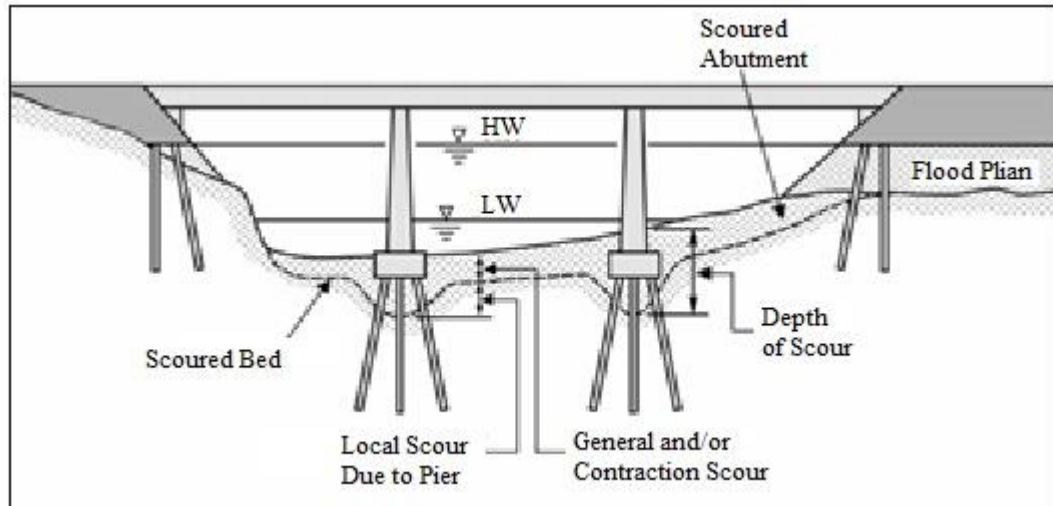


Figure 1.2 Types of scour at a bridge maiden (Robert et al., 2006)

1.3 Study Objective

The object of this thesis is to perform a numerical simulation based on an experimental study by (Adnan et al., 2015) which initially held to find a new bridge pier shape which will be economic and reduce local scour upstream and downstream of the pier. In addition, results will be compared to the experimental research to see the suitability of the Flow-3D software for studying scouring phenomena. The study objective summary is given below:

1. To study the chief explanations of scouring phenomenon.
2. To realize the mechanism of scouring around Bridge Pier.
3. To study the possibility of scouring treatment around Bridge pier.
4. To find a new bridge pier shape that minimizes scouring problem.
5. And also checking the accuracy of numerical simulation through the comparison of the laboratory and Flow-3D results.

1.4 Outline of Thesis

This thesis consists of five chapters. Summary of each chapter are given as below:

Chapter 1 Introduction:

Presenting a brief history of scour problem around bridge pier and explaining different types of scouring terminology, furthermore clarifying the study objective and the outline of the thesis.

Chapter 2 Literature Review:

This chapter covered earlier efforts that deal with, types of scouring, in general, sediment transport around bridge piers, the effect of the bridge pier shape and geometry on scouring reduction previous CFD modeling for studying scouring and general previous study on scouring problem.

Chapter 3 Experimental Setup and Methodology:

This chapter gives an explanation of both experimental and CFD modeling technique and procedures involving mesh setup, identifying boundary conditions and physical parameters.

Chapter 4 Results:

The chapter consists of result comparison for both experimental and Flow-3D model. Also, discussions of results, analysis of water surface profiles, flow velocity and turbulent field around different pier shapes.

Chapter 5 Conclusions and Recommendations:

This chapter covers the principle deductions drawn from both study and gives recommendations for forthcoming works.

CHAPTER 2

LITERATURE REVIEW

2.1 Introduction

Numerous theoretical methods, experimental researches, and numerical investigations have been extensively applied to describe the nature of turbulent flow field and local scouring around hydraulic structures. This chapter consists of a general understanding about scour phenomena and includes a brief review of the previous studies.

2.2 Scour types

A river flow will be contracted by the bridge while founding additional constructions such as abutments and piers. The amount of sediment transport increases in a constricted channel because of the increase in flow velocities. Chang (1992) described scour as the subtraction of material by water flowing in the river. Similarly, according to Breusers et al. (1977) scour is developed after water flow in rivers by a natural process. Scour can be generally categorized by way of general scouring, local scouring and contraction scouring. Types of Scour can have below descriptions as Aliba (2006) states.

2.2.1 General scour

Can happen irrespective of whether a river obstruction is existing or not; which consists of the overall lowering of the channel bed along the longitudinal profile.

General scour takes place when the river hydrology undergoes a change which leads to degradation of the channel bed. Human induced general scour can be caused by dam construction and streambed mining. Over-all scour can similarly take place over short time periods as an effect of flooding or seasonal freshet procedures.

2.2.2 Localized scour

Local scouring consists of the elimination of sediment around the base of pier structures such as bridge piers and abutments and it is directly related to the presence of a river obstruction. When water flow come across a bridge pier or abutment, the flow is directed downward to the river bed and lengthways the sides of the obstruction (Diab et al., 2010). The downward flow leads to transport of sediments away from the base of the bridge assembly.

2.2.3 Contraction scour

It takes place after the river channel is constricted either by natural (landslide) or human means such as a bridge. When the flow area is reduced by hydraulic structures, the average velocity of flow and shear stress on the river bed increase in which then the erosive forces acting upon the river bed also increase (Ozalp, 2013). After erosion increases it moves the bed material from the contracted section till equilibrium state is reached. Bridges that cause a reduction of the channel area are likely to have greater flow velocities and higher scour depths (Zevenbergen et al., 2012). In conditions where the contraction scour estimated depths are too big, Rate of scour can be reduced via increasing the crossing length of the bridge.

2.2.4 Live-bed scour

when incoming flow is carrying a significant sediment load and sediment is transported into the scour depression all the while local flow fields are also removing sediment from the scour hole. Live-bed scour generally occurs in natural river systems and also in recirculating flumes. Flumes typically do not have upstream sediment being deposited in the scour hole from incoming flow so live-bed scour does not happen.

2.2.5 Clear water scour

This hardly happens in active river channels; Which takes place when there is no upstream amount of sediment and when there is no sediment carriage into the scour hole but somewhat only sediment transferences out of the scour hole.

2.3 Sediment transport around bridge piers

In the literature, its known that flow form around a bridge pier in 4 different shapes: The down-flow, horseshoe vortex, bow wave and the wake vortices. Each form can be described as below.

2.3.1 Down-flow at the pier face

As the river flow hits the piers the velocity of flow is minimized until it reaches zero upon contacting the pier nose and leads to the increases in the overall channel depth. The approach velocity and pier shape can cause increase the flow depth (Yanmaz, 2002). When the velocity of flow decreases in the direction of the river bed the flow pressure also decreases, causing a decrease in the resulting pressure rise at the pier

nose from the water surface in the direction of the channel bed. This pressure gradient located on the pier nose generates down-flow at the bridge pier nose.

2.3.2 Horseshoe vortex

Because of the shape of the vortex, flow around a pier is frequently denoted to in the literature by means of the ‘horseshoe vortex’ (Zhao et al., 2010). The horseshoe vortex system is naturally shaped after a scour hole is produced (Ozalp, 2013). The Horseshoe vortex system takes place when the downward flow interacts by the incoming river flow as shown in Figure 3.1. The vortex flow at that point moves lengthways of the pier sides downstream. Strength of the horseshoe vortex relies on the geometry of pier and degree of turbulent flow (Yanmaz, 2002).

2.3.3 Bow waves

The bow wave arises at the water surface nearly at the face of the pier nose. It initiates from the increase in water depth as the approach flow hits the pier face and a stagnation point is created. Richardson and Davis (2001) found that for small depths of flow the bow wave causes those vortices to become weaker and leads to a decrease in scour depth.

2.3.4 Wake vortex

Wake vortices form as flow separation occurs as flow passes the sides of a pier, (Figure 2.1). These wake vortices similarly contribute to erosion of sediment around the bridge pier. Wake vortices are moved downstream via the approach flow and lead into transport sediment that is previously entrained by the down-flow and horseshoe vortex (Melville and Coleman, 2000).

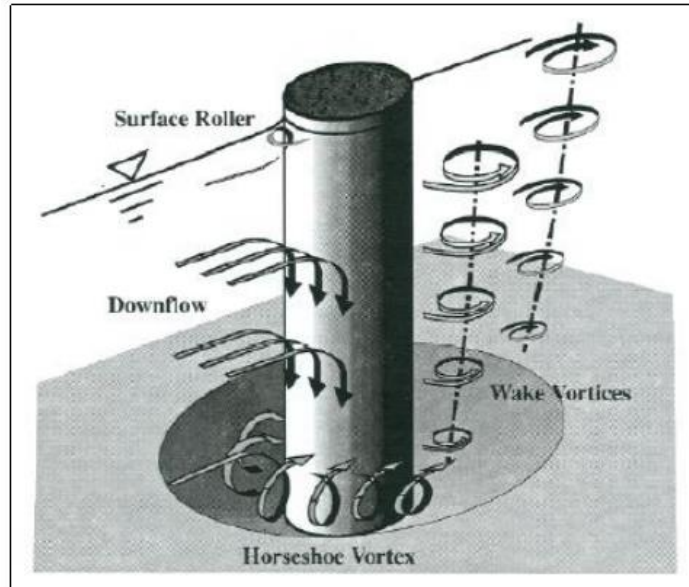


Figure 2.1 Flow pattern around circular pier (Melville and Coleman, 2000)

The chief mechanism that causes scour at bridge piers is subsequent horseshoe vortices that form on the bed of the scour hole from the down-flow (Muzzammile et al., 2004). The down-flow influences the channel bed and carries sediment past the pier base which lead to scour hole formation. Just underneath the natural bed level the down-flow strength reaches an extreme (Alabi, 2006). When the down-flow reaches the channel bed it interacts with the approaching flow and a complex vortex system develops. As shown Figure 2.1, flow past the sides of the cylinder separates and wake vortices are shaped. The wake and horseshoe vortices are both erode sediment from the pier base. Sediment deposition is common at the pier downstream side as the wake vortices strength is minimized with downstream distance (Richardson and Davies, 1995).

2.4 Effect of the shape of the pier

Tison (1961) presented advanced study and showed that scour around bridge piers possibly influenced by the streamlines curvature. Pier shapes categorized in two types according to Shen et al. (1969):

(1) Blunt-nosed pier which have a very strong system of horseshoe vortex then accordingly location of maximum scour depth is positioned at the pier upstream face. Geometry and shape of the piers at upstream face would have great impact on the depth of scour, besides that shape of the pier downstream also pier length must have the least influence when placed toward the flow using blunt-nosed pier.

(2) Sharp-nosed pier has a very weak system of horseshoe vortex and the location of maximum depth of scour takes place adjacent to the downstream face of the pier. Laursen and Toch, 1956 stated that for lengthy piers, facing an angle of attack strongly the location of maximum depths of scour moves towards the downstream and positioned near the pier end.

It is important to study the effect of the pier shape on scour depth. Many advanced researches held by Rehbock (1921), Yarnell and Nagler (1931), Laursen and Toch (1956), Chabert and Engeldinger (1956), Romita (1960), Varzeliotis (1960), Paintal and Garde (1965) and Shen and Schneider (1970). In 1956 Chabert and Engeldinger studied scour around six different shapes of piers (given in Figure 2.2 and Figure 2.3). The study results revealed that (i) pier shapes from group 1 which include pier shapes numbered as 1, 2, 4 and 6 all have nearly an equal maximum depths of scour for similarly the same conditions of flow; (ii) For the pier shape 3 the maximum depths of scour were between 33% to 86% as compared to the identical equivalent

velocities of flow from Group 1 (having higher depth ratios of scour for greater equivalent velocities of flow); lastly (iii) regarding pier shape 5 the maximum depths of scour deference was between 50% to 100% as compared to Group 1 for the same equivalent velocities of (for higher flow velocities had larger ratios of scour depths). Figure 2.3 shows the shape of the pier and angle of attack effect. It obvious from the figure that depths of scour may be reduced through streamlining of the pier having a zero angle of attack, while this benefit vanishes for angles of attack above 10° . In the case of the arrangement of 2 circular piers at a spaced 3 diameters of the pier, an exception is shaped, that shows angle of attack only have a slight impact on scour.

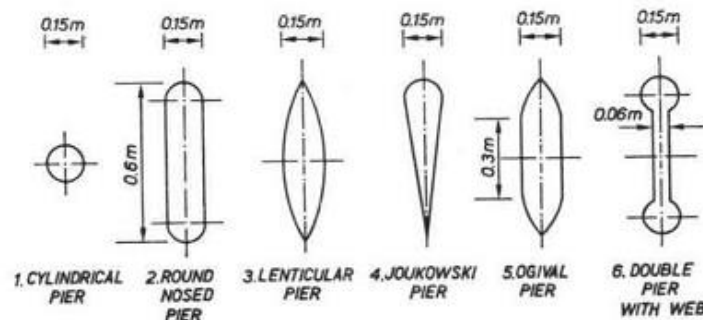


Figure 2.2 Different pier shapes tested for scour reduction (Chabert and Engeldinger, 1956)

In 1956 a study by Paintal and Garde again shows that pier rear side had no effect while upstream nose of the pier has a great influence on the phenomenon of scour. Few number of their experiments were performed on piers shaped having upstream triangular face with unlike apex angles between (15° to 180°). Their conclusion showed that with increasing apex angles maximum scour depth increased and that the pier length has a no influence on the rate maximum depths of scour for the tested pier shapes with a sediment particle size of 2.5 mm in diameter.

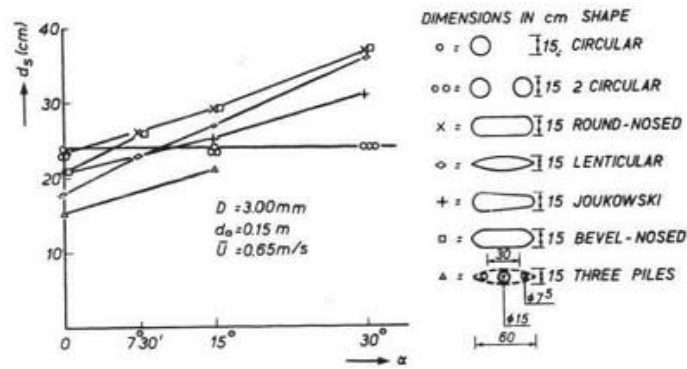


Figure 2.3 Effect of angle of attack vs the depth of scour for different pier shapes
(Chabert and Engeldinger, 1956)

Another study held by Laursen (1960) discovered that the shape coefficient (the ratio of depth of scour from a particular pier shape as compared to that of the rectangular pier) differ with the pier shape as shown in Figure. 2.4 on the other hand in 1970, Shen and Schneider tested nine pier shapes to study the effect of pier shape and their results was as following (i) A pier shape with sharp-nosed pier and a wedge nose angle of 30° has maximum scour depth located at the piers downstream face, (ii) Piers with rectangular shape and coarsened upstream face and coarsened horizontal apron give the impression of having no influence on scour, in addition (iii) An effective device for minimizing scour (40-50%) would be a pier with rectangular shape on a plane footing mounted on piers through a vertical flange around the edge of the footing when the top of the plane footing with vertical lip is positioned at the suitable height.

From all indication, one can determine that if the circular pier shape or the round-nosed pier shape is taken as a reference, scour depth reduction about 25% can be acquired by streamlining the pier, even though for angles of attack higher than 10° to

15° this good influence vanishes. Alternatively, comparing rectangular pier with the reference pier gives 20 to 40% larger scour.







NOSE FORM	LENGTH-WIDTH	SHAPE	SHAPE COEFFICIENT
RECTANGULAR			1.00
SEMICIRCULAR			0.90
ELLIPTIC	2:1		0.80
	3:1		0.75
LENTICULAR	2:1		0.80
	3:1		0.70

Figure 2.4 Shape coefficient (ratio of depth of scour of a specific pier shape according to a rectangular pier) (Laursen, 1960)

2.5 CFD modeling

Olsen and Kjellesvig (1998) under a steady current investigated local scour, by means of a three-dimensional flow in addition to sediment transport model to compute fluid behavior besides the scour development. Also, previously same alike study was held by Olsen and Melaaen (1993) to investigate in detail local scouring phenomenon. Roulund et al. (2005) using a 3D model with the $k - \omega$ model carried out a research. The outcomes from simulation model coincided well with experimental results. However, scouring around hydraulic structures was investigated significantly, still it's supposed that the free surface to be a rigid closure. Using VOF system along with a three-dimensional numerical model Liu and Garcia (2008) studied local scouring with the free water surface. Again, in 2014 Afzal et al. via the level set method performed a three-dimensional numerical study of scouring around bridge piers. Sumer and Fredsoe (2001) accomplished different tests under

the currents and wave respectively to simulate the scour development and free surface. A perfect agreement obtained from the results with laboratory observation.

Nadeem Ahmad et al. (2015) using the REEF3D modeled a cylindrical pier in a side-by-side and a triangular arrangement for studying local scouring by means of numerical simulations. In the numerical wave tank cnoidal waves are produced and by means of the level set technique the free surface is captured. Simulations were running till steady state condition is reached. Lastly, Nadeem compared the numerical results with laboratory results shown in (Figure 2.5) good agreement is realized along with the conclusions stated in the following section from the results are noticed.

1. Scour under wave act increases by means of time till steady state is reached.
2. Bridge piers with side-by-side arrangement of the lead to a contraction development and causes more scouring between the bridge opening.
3. Piers with triangular arrangement and equal spacing among the piers decrease scour rate.
4. The triangular arrangement leads to reduction in scour depth as compared to the side-by-side arrangement of the piers.

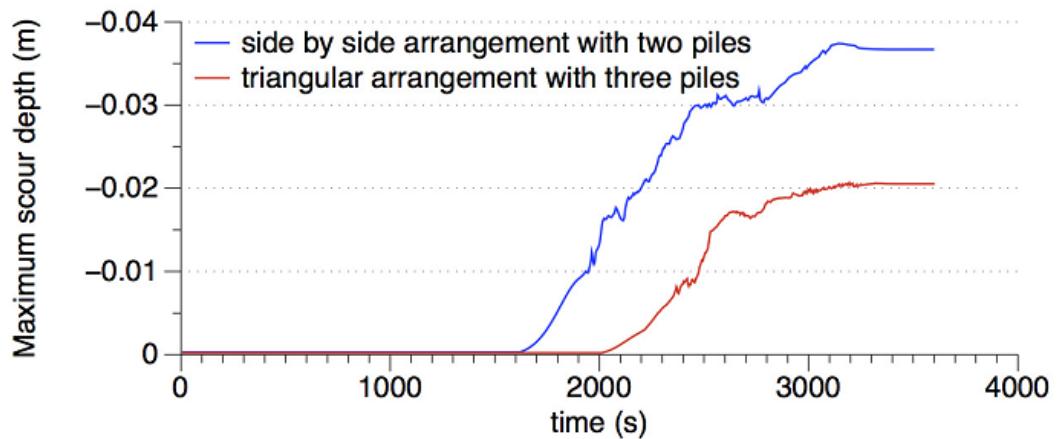


Figure 2.5 Time-based variation of the local scour around the side-by-side arrangement compared to triangular arrangement of the piers (Nadeem et al. 2015)

Vasquez and Walsh (2009) stated the qualitative simulations of local scour using the numerical modeling by Flow-3D in complex bridge piers geometry under tidal current. A complex pier consists of a large pile cap and 10 cylindrical bridge piles were used to calculate the early stages of scouring development. The results from Flow-3D showed that the software is able to properly reproduced the predictable interface between the bridge piers. Similarly, a numerical model under tidal flow reversal was used to simulate scour in a 3-pier assembly. A good agreement with measurements stated in the literature observed from the outcomes, representing that Flow-3D software is a powerful hydraulic design tool for complex piers facing many different flow states. The outcomes also stated that its doubtless the first CFD commercial model with abilities to model local scour in complex structures without the typical limits of structured boundary-fitted grids will be Flow-3D software. The software was able to properly forecast the interface between the piers, after its applied to a complex pier made of a large pile cap and several bridge piers, representing its power as a design tool for actual engineering applications. The software displayed from high standard simulations of an ideal 3-pier assembly with clear-water tidal flow, that the depth of scour reduces under tidal circumstances with

reversing the flow related to that of unidirectional stream with the similar peak velocity. Those numerical outcomes agree with experimental facts. However, an extra study by means of finer grids is required to quantitatively validate the model.

In the meantime, the key practical limitation of CFD models and Flow-3D software is the computational time needed. Because if modeling of the structure required a very large grid, excessive quantity of computational time is needed in calculation of long-term equilibrium scour, which is much greater than that required for running an experimental investigation.

HEC-18 which is developed by Federal Highway Administration. The guidelines of HEC-18 recommend the usage of Froehlich's (1989) equations of local abutment scour which were advanced by means of retreating examination of experimental tests in rectangular channel geometry. Even though, Sturm (1999) presented that Froehlich's formula over-estimates his experimental data for scour around abutment in a multiple channel since Froehlich's equation is founded on ideal experiments in rectangular channel geometries.

As HEC-18 usually used in the calculation of local scour frequently, suggests that the local scour is separate than contraction scour, and the total depth of scour can be calculated through the addition of local scour and contraction scour depths which calculated independently.

Niezgoda and Johnson (1999) investigated some Pennsylvania bridges via ABSCOUR software to conclude its performance. ABSCOUR is a software package developed by the (MDSHA) Maryland State Highway Administration used for scouring study at abutment designed for small and severely contracted bridges.

Computing scour depth at small and severely contracted bridges with ABSCOUR were more feasible than using HEC-18 equations of Laursen. Table 2.1. shows that the ABSCOUR scour depth of 4.18 m gives a better approximation than that of HEC-18 results as compared to the scour depth of 2.25 m from field results. Also, as can be seen in Table 2.6 the results of ABSCOUR simulations at other locations were moderately close to the scour depth measured from field observations. The study reveals that scouring prediction by ABSCOUR software at bridges contracted severely, agrees in a good manner with real life scour predictions.

Table 2.1 Numerical and measured depth of scour comparison at Pennsylvania bridge (Niezgoda, 1999)

Method	Location		
	Piney-creek	Brush Run	Little Creek
Field Scour Depth (m)	2.25	1.92	3.05
HEC-18 (m)	7.62	-	-
ABSCOUR (m)	4.18	2.13	3.81

2.6 Studies about bridge pier scour in general

Ataie-Ashtiani and Beheshti (2006) studied effects of group piles assembly (without a pile cap) local scour. In their laboratory observation, they concluded that for small spacing between the bridge piers in a side-by-side order, development of scour depth will increase by a mean of 50%; whereas for a tandem assembly, scour rate increases in the upstream pier pile whereas scouring decreases in the downstream protected pier.

Manouchehr et al. (2010), carried out a study around two and three pile groups of with circular collar for the case of clear-water flow over uniform sediment particles, for the purpose of scouring reduction. Using groups of two and three bridge piers through experiments. The collars efficiency, with respect to different pier sizes and

spaces among the piles, is calculated. The result showed that collar reduces depth of scour in downstream piles more than the upstream one. Correspondingly, increasing the spacing among the piers causes the area between the piers that is without protection to be eroded away causing a larger depth of scour at the downstream piles.

An experimental study of local scour under tidal flow conditions was carried out by Escarameia (1998), he used single circular and rectangular piers to investigate the effect of reversal on flow direction, tidal cycle interval, depth of water, pier shape, and size of sediment on local scouring phenomenon. The results showed that local scour depth is not influenced by sediment size. In tidal conditions the maximum depth of scour stayed continuously lesser than that of equilibrium depth of scour for unidirectional current; in case of clear-water scour (no bedforms were existing). Piers having rectangular shape found to reduce scour depths about 10 to 14% when compared to piers with square geometry. Scour holes in square piers shaped at both upstream and downstream of the pier throughout the tidal cycle integrate, while for the rectangular pier does not occur.

May and Escarameia (2002) using square and sinusoidal tides, studied the time-based development of local scour under tidal circumstances. They determined that the equilibrium sediment scour in clear-water scouring at hydraulic structures in tidal streams can be fewer than scouring with unidirectional flow significantly. But, with sediment movement (in live-bed) scour hole formation, the equilibrium scour depths are expected to not differ too much as compared to the unidirectional flow value because of the earlier formation of scour holes in each tidal cycle and as a result of the development of dunes all around the structure constructed in the river channel.

An experimental study held by Margheritini et al. (2006) for investigating local scour with sediment movement (live-bed conditions) around large diameter bridge piers in unidirectional and tidal flow condition. The concluding equilibrium scour was similar for both cases. Symmetrical scour holes in tidal flow condition was developed, having a circular form and a volume bigger as compared to the unidirectional scour hole development.

2.7 Initial motion of sediment particles

Initial motion of sediment arises when flow intensity in a channel is barely adequate to drag bed particles. The fluid hydrodynamic forces acting on the particles are responsible for their motion (Kanellopoulos, 1998). Since sediment is transported along a riverbed in a complex manner, it can be challenging to explain the flow conditions in which sediment will move. For this reason, studies concentrate on the flow conditions adjacent to the incipient motion of sediment particles. As shown in Figure 2.6, the forces acting on a sediment particle are mainly composed of four forces: F_L denotes the lift force (buoyance), F_W represents the force downward from the submerged weight, F_R is the resistance force F_D is the drag force.

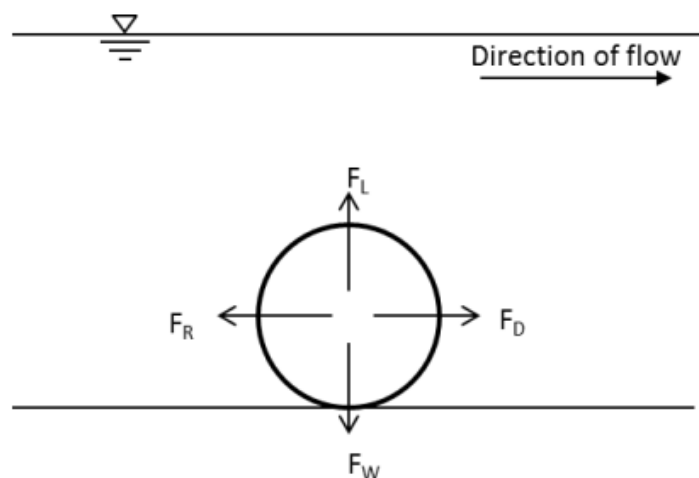


Figure 2.6 The main forces acting on a sediment particle and their direction.

In order for initial motion to take place one of the following conditions must be satisfied:

$$F_D = F_R \quad (2.1)$$

$$F_L = F_W \quad (2.2)$$

Many variables cause the lift, drag, resistance and weight, forces acting on a sediment grain. Shields, in 1936 was the first to develop a relationship so as to satisfy the conditions for initial motion between hydraulic variables and sediment characteristics. Shields by using dimensional analysis studied circumstances in which bed particles are stable but on the edge of being moved. Shields figured out that the critical conditions in which sediment is near to become entrained can be found by involving the critical Shields value (τ_c^*) and the shear Reynolds number (Re^*). The critical Shields value, similarly named the dimensionless shear stress, is given by the following relation:

$$\tau_c^* = \frac{\tau_{bc}}{(\rho_s - \rho)gD} \quad (2.3)$$

where $\tau_{bc} = \rho U^*c_2$ = critical bed shear stress for initiation of motion of the particles, U^*c is the critical shear velocity of flow, $(\rho_s - \rho)$ is the soil particle of and water density correspondingly, g and D is gravity and the diameter size of the soil particles respectively.

Re is Reynolds number, which is a dimensionless quantity that defines the inertial forces to viscous forces ratio. The Reynolds number is mainly used to describe

whether there is laminar or turbulent flow. At low Reynolds numbers while there are dominant viscous forces, laminar flows take place, whereas at high Reynolds numbers where inertial forces are dominant turbulent flows are taking place. The Reynolds number can also be adapted to investigate the initial motion of sediment particle through the particle Reynolds number. The particle Reynolds number is specified as follows:

$$R_e = \left(\frac{U d_{50}}{\nu} \right) \quad (2.4)$$

U is the flow velocity, d_{50} is the median particle diameter of the sediments and ν is the kinetic viscosity of fluid. When studying initial motion, the shear Reynolds number R_* is dedicated to as it uses the shear velocity and is written as:

$$R_* = \left(\frac{U_* D_{50}}{\nu} \right) \quad (2.5)$$

where U_* is the shear velocity of flow. The graphical relationship produced between the dimensionless shear stress ($\tau_* c$), and the shear Reynolds number (R_*) is devoted to as the Shields diagram which characterizes values in which incipient motion of sediment happen. The relationship is dimensionless therefore that the resisting forces and the driving forces of particle motion can be compared (particle size, particle density).

The initial motion of sediment not only depends on hydraulic variables but similarly on the characteristics of the bed material also. Initial motion of non-uniform particles is more complex than uniform particles of sediment meanwhile sediment in motion is influenced by means of the grain shape, interactions between grains and alignment

in the channel bed. The Froude number that is used to determine the resistance of an object flowing through water denotes the ratio of inertial forces to gravitational forces of the fluid. The larger the Froude number, the larger the resistance applied on water flow by the river bed material. The Froude number is specified by:

$$F_r = \left(\frac{U}{\sqrt{gh}} \right) \quad (2.6)$$

where h is the depth of flow. In order to use the Froude number to observe transport of bed material, the dimensionless form of the Froude number can be used. The densimetric Froude number is the ratio of sand inertial forces to the submerged weight of the sand grain. The densimetric Froude number is given as:

$$F_o = \frac{U}{\sqrt{\frac{gd_{50}(\rho_s - \rho)}{\rho}}} \quad (2.7)$$

where d_{50} is the bed sediment median grain size. Even though in the literature initial motion of uniform sediment has been studied (Buffington and Montgomery, 1997; Kanellopoulos, 1998; Andrey and Gareth, 2000; Vollmer and Kleinhans, 2007; Beheshti and Ataie, 2008), limited studies that observe the initial motion are made for a non-uniform bed material, Xu and Yu (2008) established a study on incipient velocity formulation based upon the uplift and drag forces and confirmation of the formula with field data. The authors discovered that the needed incipient velocity for coarse non-uniform particles was fewer than the incipient velocity for uniform

sediment. Additionally, they calculated that the incipient velocity was larger for fine particles for non-uniform sediment than that for uniform sediment.



CHAPTER 3

MODEL SETUP

3.1 Introduction

In this work, a 3D numerical model of sediment scours simulated based on a experimental study by Adnan et al. (2015). The experimental works were performed in hydraulics laboratory at the Gaziantep University at civil engineering department, and the numerical model is simulated using Flow-3D software. The following section includes a complete detail of performed work.

3.2 Experimental Procedure

Figure 3.1 shows the experimental setup of Adnan et al. (2015). The experiments were performed in a recirculating flume having the following dimensions 12 m in length, 0.8 m width, and 0.9 m height. The channel sides of the flume were made of smooth glasses. The soil section part composed of 3 m long with depth of 0.2 m of soil shown in Figure 3.1. Magnetic flow meter instrument which is installed in the pipe system was used to measure the flume discharge, placed right before the channel inlet. Laser meter was used for measuring scour hole dimensions and the bed soil elevation of the tested section. The instrument installed on the upper side of the flume fence on a manually moving carriage move smoothly on rails.

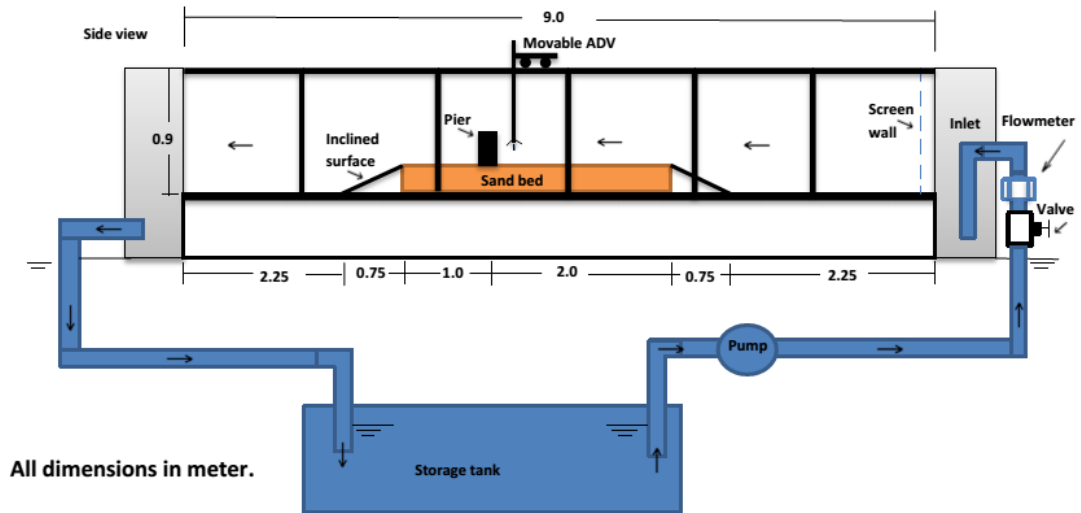


Figure 3.1 Schematic layout of the flume (Adnan et al., 2015).

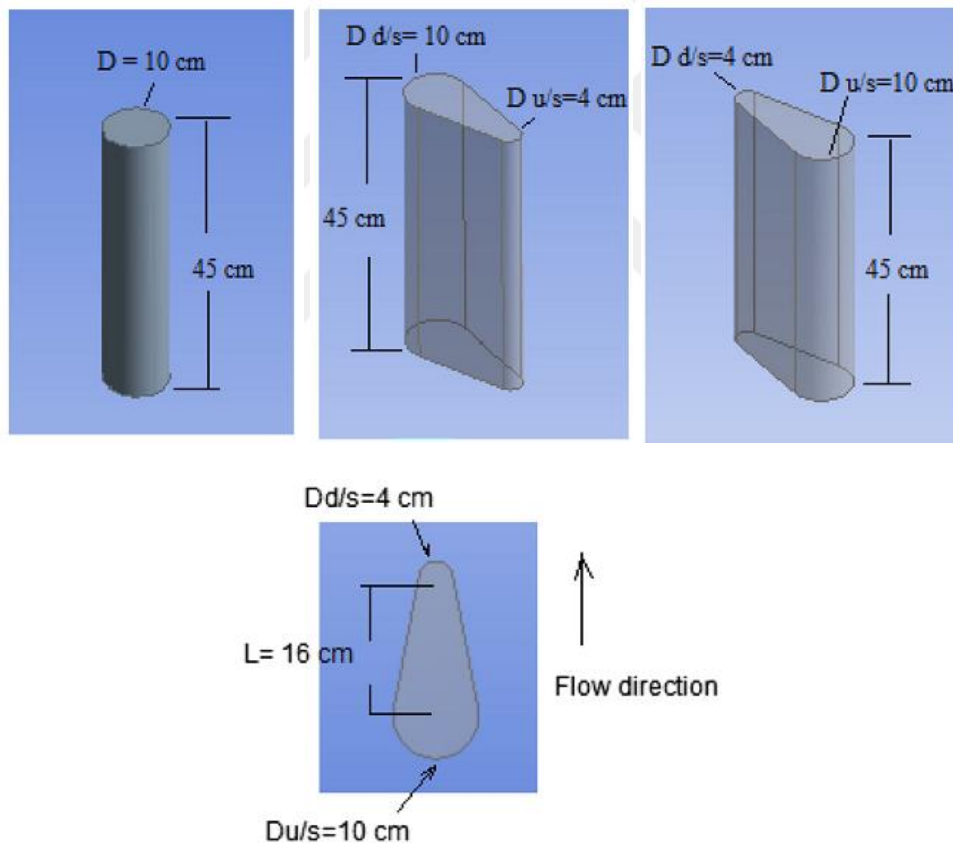


Figure 3.2 Shape and dimensions of tested bridge piers (Adnan et al., 2015)

Three different models of piers were used in the tests, (1) circular pier, (2) upstream-facing round nosed pier (US-FRNP) (10- 4) cm (3). Downstream-facing round nosed pier (DS-FRNP) (4- 10) cm. Piers were made from thermo-stone and painted for the

purpose of reduction of surface roughness of these piers. Figure 3.2 shows shape and dimensions of tested piers. The pier was placed on the center line of the flume at all cases, and the coordinates of the pier centreline kept constant for all three cases. To ensure the inter-comparison of measured contour profiles.

Choosing the pier diameter was based on Ettema (1980) study which states that the bed soil particle size has no effect on the depth of scouring as long as the width of the pier to the ratio of grain size exceeds a value of about 50. To omit effect of size of the sediment on the scour depth the ratios between 50-68 for all the piers used in the study to satisfy the criteria of Ettema.

The soil material that has been used in the study was categorised after a series of tests including a mechanical sieve analysis and a specific gravity test were performed. Test outcome presented that section is composed of sediment with median particle size $d_{50} = 1.45\text{mm}$, standard deviation, $\sigma_g = 3.16$ and the specific gravity of $2.65 \text{ (g/cm}^3\text{)}$; Fig.3.3 presents the sieve analysis of the bed material.

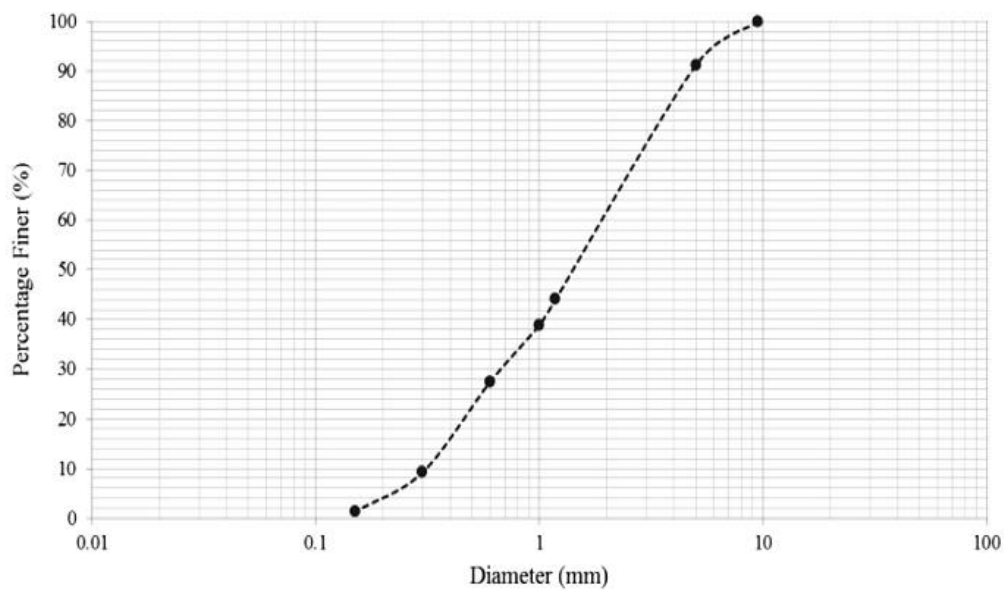


Figure 3.3 Grain size distributions

3.3 The Numerical Modelling

Numerous 3D numerical simulations have been efficiently practiced to study local scour in a single cylindrical pier after the early study of Olsen and Melaan (1993), (see evaluation of Roulund et al. (2005)). However, there is still a significant gap in the area of local scour for non-uniform pier shape numerically. This is because, almost all models are founded on structured curvilinear boundary-fitted grids that have problems to accurately model the geometry of non-uniform pier shapes. Computational time is another chief restriction, that is expressively higher than the time needed to complete a local scour test in an experimental investigation. Yet, when computer speed is predictable to increase still more numerical models can offer valued information and have a countless potential for the future. In this study a numerical modeling was created using Flow-3D software, which developed by Flow Science Incorporation.

Flow-3D software is a commercial CFD package with superior modules proposed for hydraulic engineering studies. The software uses a structured orthogonal grid and also, by the application of the fractional area volume method (FAVOR) can model complicated geometries. Volume-of-Fluid (VOF) method is used to model free surface flow (Hirt and Nichols, 1981) tracking air and fluid or fluid with fluid boundaries. The method of tracking has the capability to records the volume of fluid in every single rectangular cell and disregard the air surrounding the flowing water, which allows the numerical model to generate a sharp edge between the flowing water and the surrounding air without the usage the fine meshes essential in other CFD software packages. The software is a very powerful in modelling local scour, as described by Brethour (2001). Flow-3D solves the transient three-dimensional Navier-Stokes equations on a structured grid domain, and the model has the facility

of automatically select time-step size, graphical post-processing in a short time, and many other superior features facilities which will be discussed in the following sections.

In the numerical facilities of the software, computing of results are done using numerous implicit and explicit solver options and finite difference solution scheme is used for utilization. Inside the grid the geometry is defined by calculating the fractional face areas and fractional volumes of each element that are faced by an obstacle. Other choices that make the software appropriate for modelling hydraulic structures, is the use of a multiple and nested meshes, and the re-run capability existing in Flow-3D. The solid boundary edges are simulated with (FAVOR) method the fractional area-volume obstacle representation for modelling solid obstacles such as piers, that provides the software to use completely structured grid. While other CFD software's possibly will need the usage of the deformed grid to simulate flow over and around structures especially bridge piers. Furthermore, the program accounts for cells which are not only wet or dry through defining their small impact on the flow in the domain.

With all the great features that software has a comparative decent simulation of flow of composite geometries is easy to attained from moderately coarse meshing sizes. For this study, three pier models were resolved nicely with the software. The program includes some turbulent closures by means of many well-advanced and generally accepted numerical systems universally (Launder and Spalding 1972; Rodi 1980; Abbot and Basco 1989; Shaw 1992) that consist of Prandtl's mixing length option, single equation turbulent energy (k) option, two equation($k - \epsilon$) options, Renormalization-Group (RNG) option, lastly Large Eddy Simulation closure

schemes (LES). Modelling flow field around bridge piers with Flow-3D, a well-developed turbulence closure model is required. Through Kolomogorov- Prandtl expression (Flow Science, 2009), Kinematic turbulent viscosity is related with turbulent kinetic energy, k , and the turbulent dissipation, ϵ .

3.4 Sediment Scour parameters and modelling

The experiment was simulated with Flow-3D. Clear water scour around a row of different pier models is simulated. Three different piers named (Circular pier D=10 cm), (UFRNP 10-4 cm) and (DFRNP 4-10 cm) are used. The upstream flow which has maximum velocity of 0.58 m/s, and it is directed to the cylinders. The bed material is composed of sand of median size of ($d=1.45$ mm) with mass density and scour parameters: mass density = 2650 kg/cm^3 , critical Shields parameter = 0.05, entrainment coefficient =0.018, and bedload coefficient = 8.0. The critical packing fraction is 0.64. The output was compared directly to the experimental results. Table 1 shows the cases that had been conducted both experimentally and simulated. All simulations were conducted on a three-dimensional single mesh block with 30,720 uniform cells, each about a 0.025 m cube.

Table 3.1 The Test conditions

Series	Cases	Q (m3/sec.)	Water depth (cm)	V (m/s)
Series 1	Circular pier	0.058	12.5	0.58
	US-FRNP	0.058	12.5	0.58
	DS-FRNP	0.058	12.5	0.58
Series 2	Circular pier	0.048	11	0.54
	US-FRNP	0.048	11	0.54
	DS-FRNP	0.048	11	0.54

US-FRNP= UPSTREAM-FACING ROUND NOSED PIER (10-4) cm.

DS-FRNP = DOWNSTREAM-FACING ROUND NOSED PIER (4-10) cm.

The sediment scours model assumes several sediment types with unlike properties such as mass density, grain size, the angle of repose, critical shear stress, and parameters intended for entrainment and transport. For instance, sand with medium and coarse particle size, also gravel can be sort into different species having different diameter in the simulation of the numerical model. For each species the model computes all the sediment transport processes together with bed load and suspended load transport also entrainment, and deposition of sediment particles.

Entrainment defined as the process of turbulent eddies removing the grains on the top of the packed bed then carry them into suspension. It occurs when the bed shear stress surpasses a threshold rate (critical shear stress). While entrained, the grains are transported by the flowing water within a specific height above the packed bed, identified as the suspended, load transport. Deposition occurs once suspended grains settle on top of the packed bed because of the collective effect of buoyancy, gravity, and friction. Bed load transport defines the sliding, hopping and rolling motions of grains lengthways the packed bed surface in reply to the shear stress exerted by fluid flow (Flow Science, 2009). Each parameter has been specified according to the model's variables.

3.4.1 Meshing setup

Figure 3.5 shows the computational domain and the mesh setup. Since the problem is symmetric in the lateral direction, the domain covers only the region at one side of the Piers. The mesh has 38400 uniform cells. At the upstream boundary of the mesh

block, simulation of turbulent flow over a flat plate is used to calculate a velocity profile.

3.4.2 Specifying Boundary Conditions

Figure 3.6 shows the boundary condition for the simulated model, as shown the upstream boundary is specified velocity and the downstream is outflow boundary while the bottom is counted as wall boundary and the top is pressure boundary with zero Fluid fraction, on the other hand the minimum y boundary condition is a symmetry boundary as only the half of the model is placed in the calculation domain so to complete the remained part.

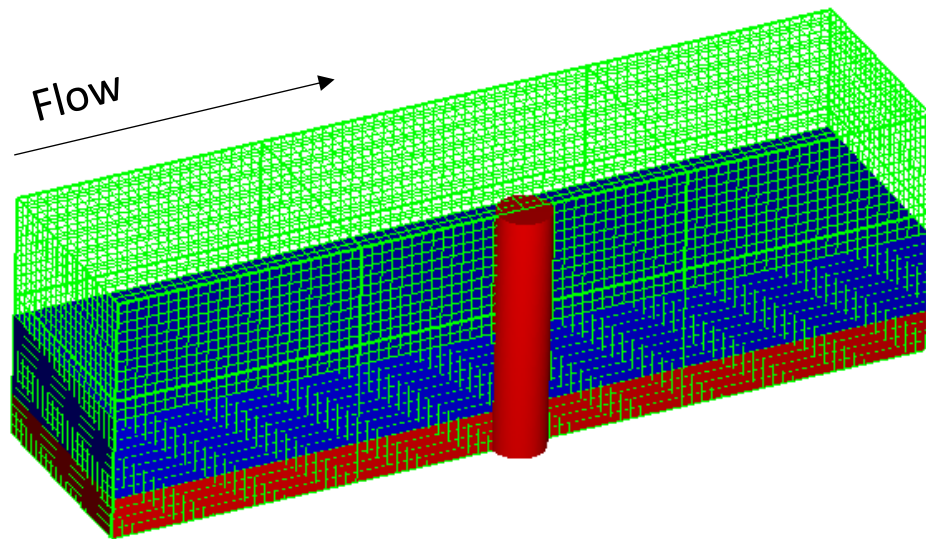


Figure 3.5 Computational domain and mesh setup around the Bridge pier

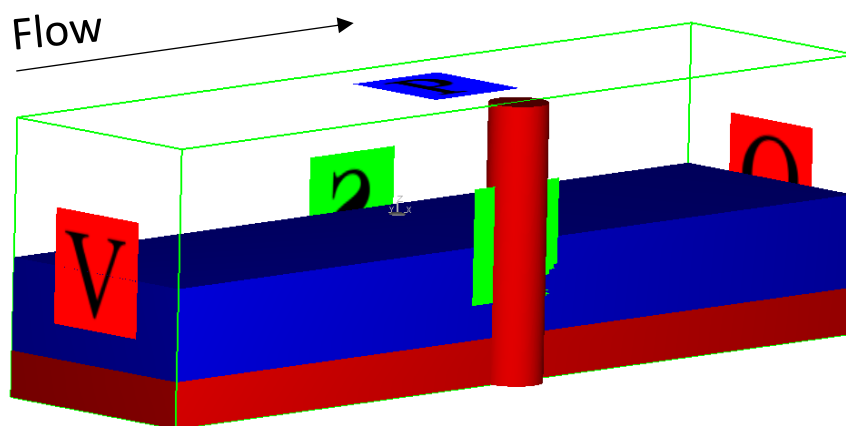


Figure 3.6 Boundary conditions

3.4.3 Physics and Numerical Options

Different physical options available in Flow-3D, for sediment scour there some specified parameter needs to be taken into consideration most important ones include: sediment scour, gravity and non-inertial reference frame, viscosity and turbulence, each of the mentioned physics option also include other different option for example in turbulence option there is three different choices which they are (two equation ($K-e$)) model, (RNG) model renormalized group model in addition to the large eddy simulation model. In this study (RNG) model chosen for simulation purpose. This is because results from different studies of turbulence models reveals that the (RNG) model is a good choice for predictions of the mean flow field and are close to the laboratory results (Anu and Jennifer, 2011).

The RNG $k-e$ model was derived expending a hard statistical method (called renormalization group theory). It is related in formula to the standard $k-e$ model, but consist of the subsequent improvements:

- The RNG theory has an additional term in its e equation that considerably progresses the precision for speedily strained flows.
- The influence of eddy on turbulence is involved in the RNG model, improving precision for whirling flows.
- The RNG model runs an analytical method for turbulent Prandtl numbers, while the standard $k-e$ model practises user-defined, constant values.
- Whereas the standard $k-e$ model is a high Reynolds-number model, the RNG model runs an analytically derivative differential method for active viscosity that accounts for low Reynolds-number effects.

The above features make the RNG $k-\epsilon$ theory more precise and dependable for an extensive class of flows as compared to the standard $k-\epsilon$ model Flow (Science, 2009).

The general form of $k-\epsilon$ model with and additional transport equation is solved for the turbulent dissipation e_T as:

$$\frac{\partial \epsilon_T}{\partial T} + \frac{1}{V_F} \left\{ \left(v_{\epsilon} A_x \frac{\partial \epsilon_T}{\partial x} \right) + \left(v_{\epsilon} A_y R \frac{\partial \epsilon_T}{\partial y} \right) + \frac{\partial}{\partial z} \left(w A_z \frac{\partial \epsilon_T}{\partial z} \right) \right\} = \frac{CDIS1 \cdot \epsilon_T}{\kappa_T} (P_T + CDIS3 \cdot G_T) + \text{Diff}_{\epsilon} - CDIS2 \frac{\epsilon_T^2}{k_T} \quad (3.1)$$

Where CDIS1, CDIS2, and CDIS3 are all dimensionless user-changeable parameters, and have defaults of 1.44, 1.92 and 0.2, respectively for the model.

The diffusion of dissipation, Diff_{ϵ} , is:

$$\text{Diff}_{\epsilon} = \frac{1}{V_F} \left\{ \frac{\partial}{\partial x} \left(v_{\epsilon} A_x \frac{\partial \epsilon_T}{\partial x} \right) + R \frac{\partial}{\partial y} \left(v_{\epsilon} A_y R \frac{\partial \epsilon_T}{\partial y} \right) + \frac{\partial}{\partial z} \left(v_{\epsilon} A_z \frac{\partial \epsilon_T}{\partial z} \right) + \xi \frac{v_{\epsilon} A_x \epsilon_T}{x} \right\} \quad (3.2)$$

The RNG theory uses equations related to the equations for the $k-\epsilon$ model. Yet, equation constants that are found empirically in the standard $k-\epsilon$ model are derived explicitly in the RNG theory. In general, the RNG theory has broader applicability than the standard $k-\epsilon$ model. In particular, the RNG model is known to describe small intensity turbulence flows in addition to the flows having high shear regions more precisely. Similarly, the default values of CDIS1 and CNU are unlike than those are used in the standard $k-\epsilon$ model; they are 1.42 and 0.085, respectively. CDIS2 is calculated from the turbulent kinetic energy (k_T) as well as turbulent assembly of (P_T) terms.

In wholly turbulence transport theories, the kinematic turbulent viscosity is calculated as of:

$$\mathcal{E}_{T,min} = CNU \sqrt{\frac{3}{2} \frac{k_T^{3/2}}{TLEN}} \quad (3.3)$$

Where v_T is the turbulent kinematic viscosity.



CHAPTER 4

RESULT AND DISCUSSION

4.1 Introduction

Simulated results from Flow-3D software of different pier shapes and scoured bed formation are compared with laboratory results to assess the precision of the numerical model. CFD models were run many times so as to validate the relative impact of local pier scour. In this section, results will present the comparisons of the simulated and experimental results, scour hole formation at different time, flow field variations and the velocity magnitude, also scour development with velocity distribution and the turbulent intensity at each location of the scoured bed. In this investigation, the calculated depths of scour from the experiment study and computed depths of scour from the CFD model will be compared, after that the influence of different pier shape on depth and volume of scour will be presented. Finally, the results will be discussed.

4.2. Comparison of simulated and experimental results

Table 4.1 presents the comparison of the results for both experimental and CFD results at a different time for different pier geometries and their maximum scour hole depth. The results show that Flow-3D under predicted the scour depth for the circular model, while it over predicted the scour hole depth at US-FRNP and DS-FRNP but the overall results from the Flow-3D is close to the experimental results

Table 4.1 Maximum Depth of scour for physical & numerical models

Time (min)	Discharge (l/s)	Depth of scour					
		circular pier		US-FRNP (10–4 cm)		DS-FRNP (4–10 cm)	
		Exp.	CFD	Exp.	CFD	Exp.	CFD
5	58	8.6	7.9	7.1	7.5	4.2	5.3
15	58	9.2	8.7	7.5	8.0	4.6	5.7
30	58	9.8	9.4	8	8.4	4.8	6.0
60	58	10.2	10.0	8.1	9.3	4.9	6.6
120	58	10.4	10.1	8.3	9.5	5.0	6.9
180	58	10.9	10.3	8.4	10	5.0	6.9
5	48	6.0	4.8	4.6	3.0	2.6	2.1
15	48	6.4	5.0	4.8	6.0	2.8	2.5
30	48	6.8	5.1	5.4	6.9	2.8	2.6
60	48	6.9	5.5	5.6	7.0	2.8	4.8
120	48	7.0	6.2	5.8	7.2	2.8	5.0
180	48	7.0	6.2	5.8	7.2	2.8	5.0

In the experimental investigation for discharge of 58 l/s it can be seen that the downstream facing round-nosed pier reduced depth of scour about 54% when compared to the circular pier shape also a reduction of 40% is gotten using downstream facing round-nosed pier when related to the upstream facing round-nosed pier. while for the Flow-3D model the reduction was only 36% decrease when compared to the circular bridge pier shape and only 28.5% decrease when compared to the upstream facing round-nosed bridge pier respectively. However, the Flow-3D results are not quite similar to the experimental but it gives the same conclusion for the best model. And the overall results tell us that beside the reduction in the depth of scour Figure 4.1, rate of scouring formation is also minimized in both cases. This benefit can decrease the danger of the pier failure when the floods period is small Melville and Chiew (1999).

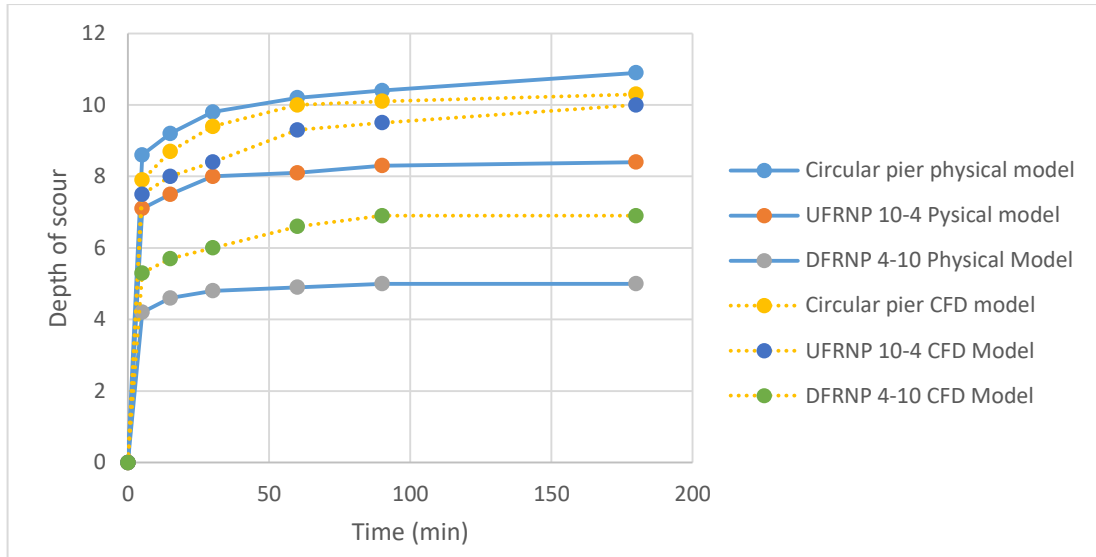
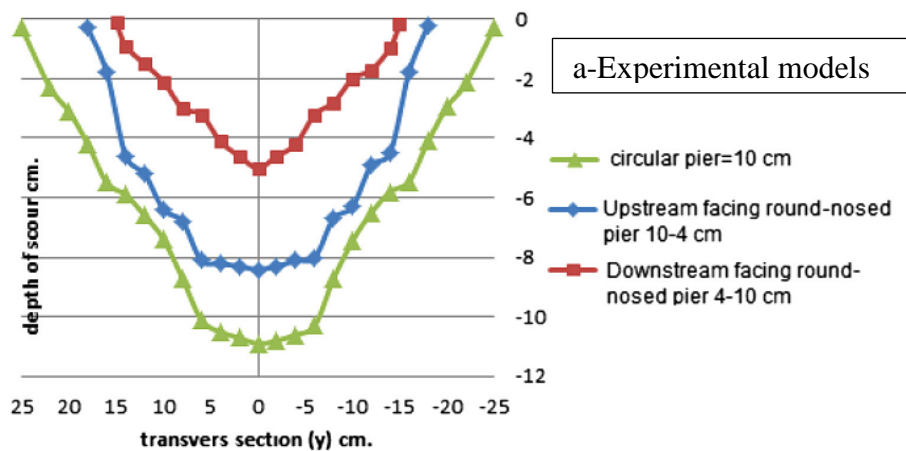
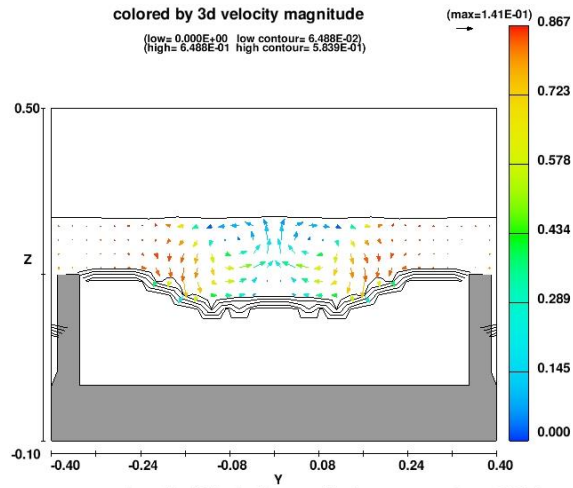


Figure 4.1 Maximum Scour hole development for experimental and CFD model of each tested pier (58 l/s)

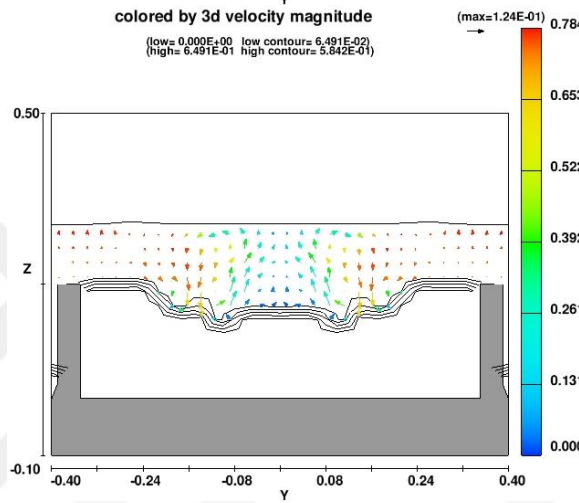
Figure 4.2 reveals the top scour holes formation of all three different bridge pier shapes. Width of the top scour hole of DS-FRNP was 20 cm or 40 % fewer than the circular pier and 6.0 cm or 17 % fewer than the US-FRNP, while for the CFD model it was 16 cm or 31% less than the circular bridge pier and 10 cm or 21 % fewer than the US-FRNP. This reveals that DS-FRNP reduced the effect of the horseshoe vortex of the down flow toward the base of pier structure.



b-1 Circular



b-2 US-FRNP 10-4



b-3 DS-FRNP 4-10

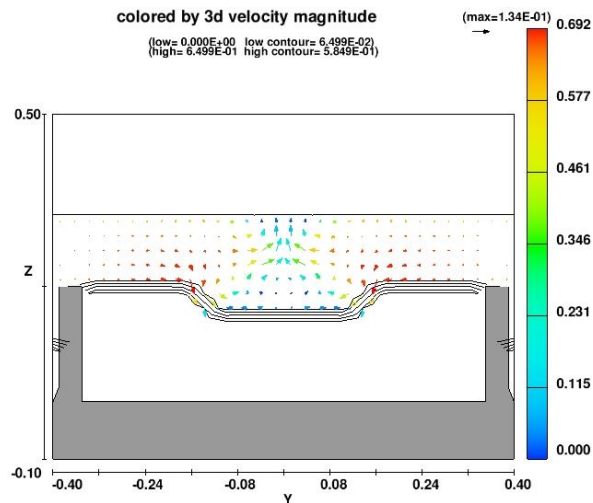
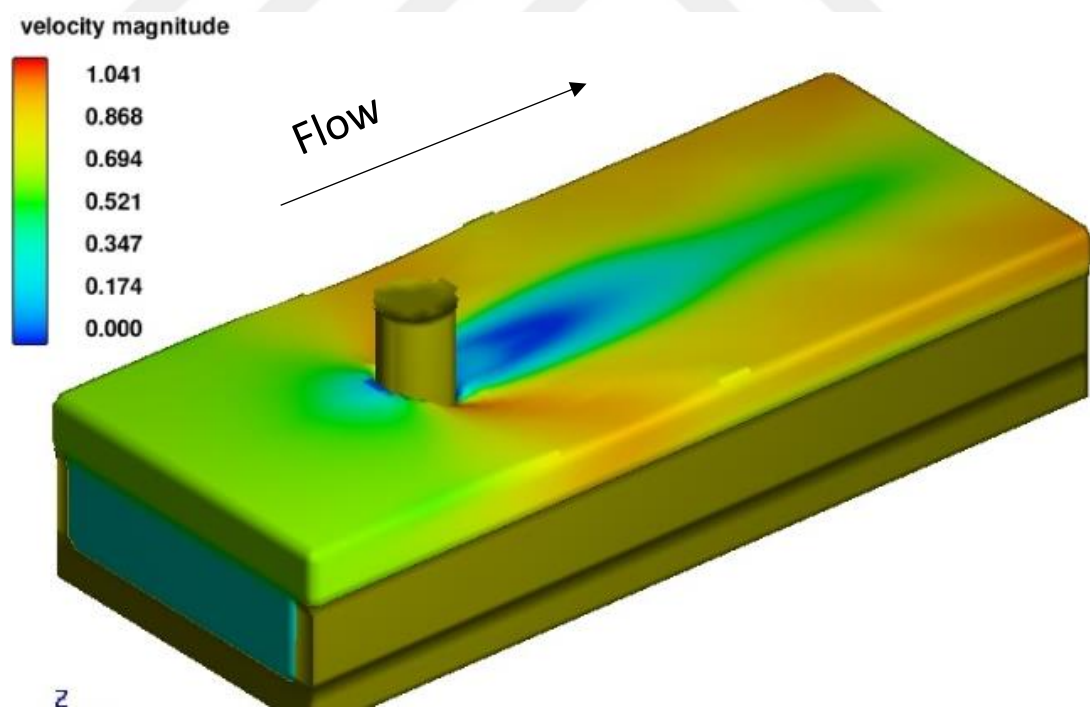


Figure 4.2 Crosswise scour holes of three different bridge piers a-Experimental models (Adnan et al, 2015) b-CFD models (b-1. circular b-2. UFRNP 10-4, b-3. DFRNP 4-10)

4.3 Flow field and velocity magnitude

Figure 4.3 shows the flow around all the models at 30 min. along with the velocity magnitude distribution at every single point in the model. From the color bar, it can be noticed that the average flow velocity in the domain is around (0.6) m/s and the velocity is higher around the piers but it decreases to a great deal immediately behind the piers, which lead to a reduction in scouring in such position. The velocity distribution at each model give and idea about the performance of each model, for example when comparing the circular pier with DS-FRNP (4-10) cm one can realize from the red colour distribution that a has high-velocity magnitude, that the DS-FRNP caused the flow to pass through a separation points and caused maximum velocity magnitude located away from both sides of pier and push the higher flow intensities to the edge of the canal model.



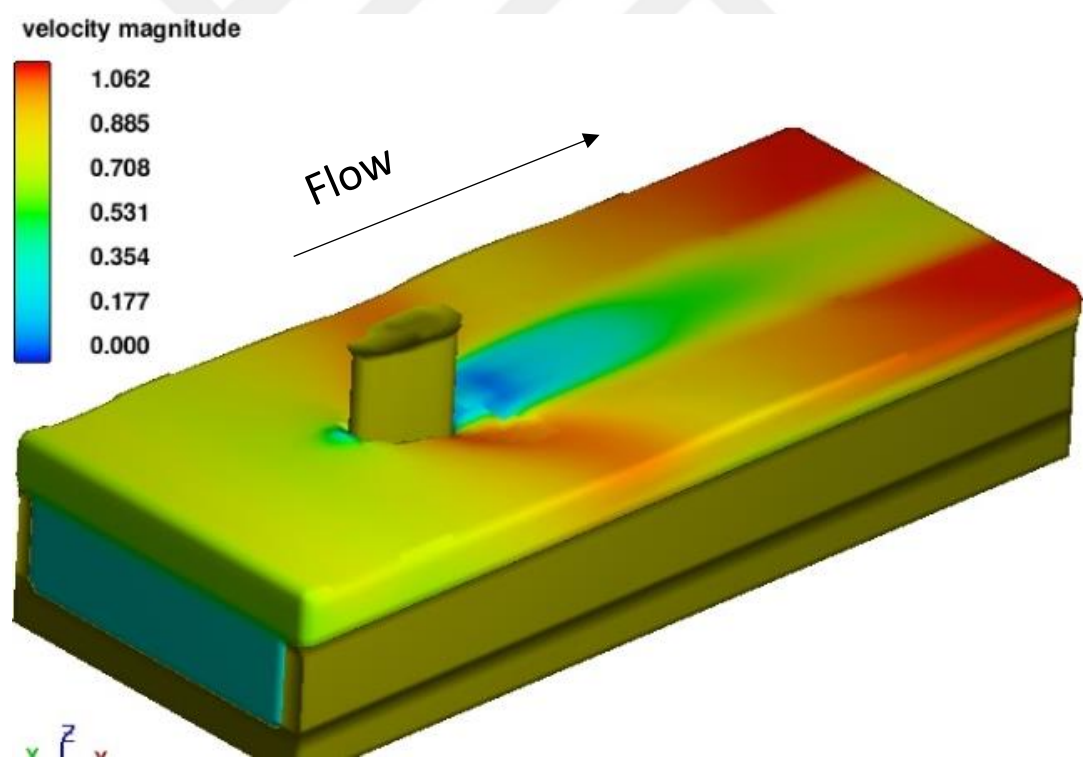
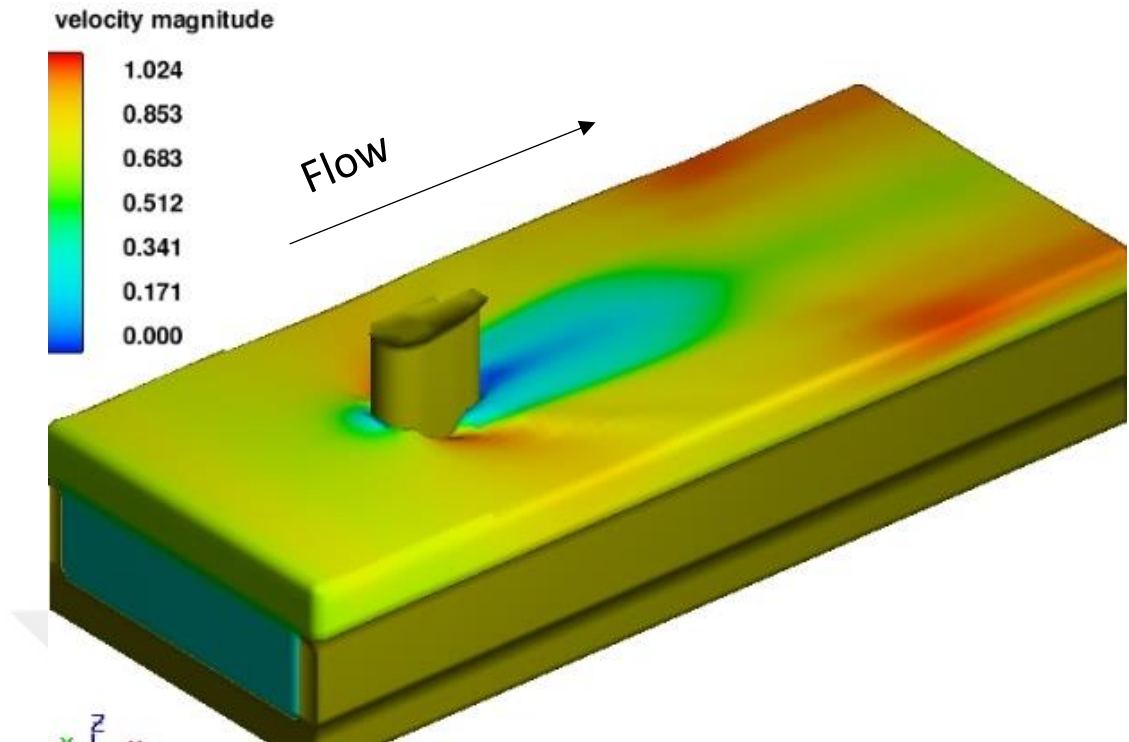


Figure 4.3 Flow around the circular pier at 15 min.

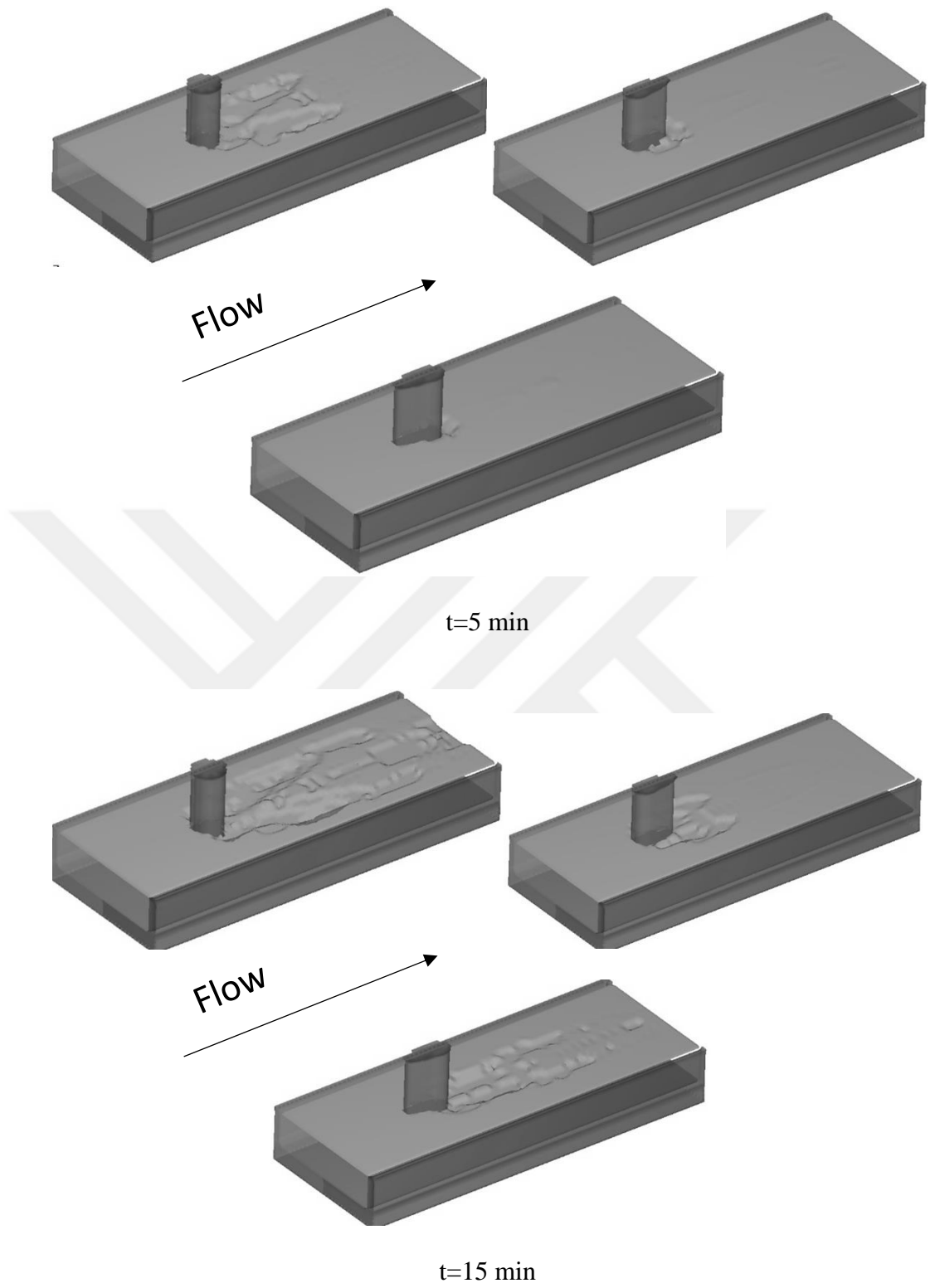
4.4 Scour development versus time

A considerable study from literature concentrates on the maximum scour depth location and rate around piers, while for the intent of bridge construction it is equally important to consider the scour volume and scouring area. In general, the maximum scours depth around a single pier develops at the nose of the pier structure; still, the location of the maximum depth of scour for different geometry and hydraulic condition does not necessarily take place at the nose of the pier structure. Because the maximum scour location is reliant on complexities of the geometry of the pier bents as well as the orientation of the piers and bridge opening to the approach flow, hydraulic parameters and sediment properties. Based on scouring contours of each pier shape for the Flow-3D modeling as shown in Figure 4.4, most occurrences of maximum depth of scour depth were developed at the lateral sides of the piers for the same flow rate. When we have weak horseshoe vortex in the system, location of maximum scour depths does not necessarily take place at the nose of the bridge pier and it moves towards the downstream end of the bridge pier structure (Shen et al. 1969), (Laursen and Toch, 1956).

In Figure 4.4 the scour holes around all the pier models and their variations with time are shown. As it can be noticed that scour hole development around the circular model is faster as compared to the other two models and the DS-FRNP is the slowest model in producing scour holes. Another point is as the time passes we can see that the scour hole top width is enlarging in a very fast procedure as compared to the other two models which show the shape and orientation effect of round-nosed pier especially for the DS-FRNP (4-10), considerable scour decrease happened at the upstream face of the bridge pier as (Adnan et al., 2015) also stated. Some other

interesting point is that from the initial stages of scouring and after time passes it can be noticed that the DS-FRNP Is deflecting the scour production away from the pier to the downstream which is another benefit to increase the life of the pier foundation against failure due to scour.

A study by Dey and Raikar in (2007) reveals that inside a scour hole area there is a higher degree of turbulence that increases as the scour hole grows bigger. Inside the scour hole there exist the horseshoe vortices along with turbulent intensities are in charge for the place of the maximum scour depth. There is also a reduction in scour depth located immediately behind the pier on the downstream side. As the flow passes the sides of the pier, the flow splits and wake vortices take place. The wake vortices are moved downstream by the approach flow and are in charge for transport of sediment that is previously entrained through the down flow and horseshoe vortex (Melville and Coleman, 2000). The strength of the wake vortices is naturally fewer than the horseshoe vortices and hence cannot transport the equal sediment load as the horseshoe vortex do. Since the wake vortices are weaker behind the pier and sediment deposition may occur downstream of the pier.



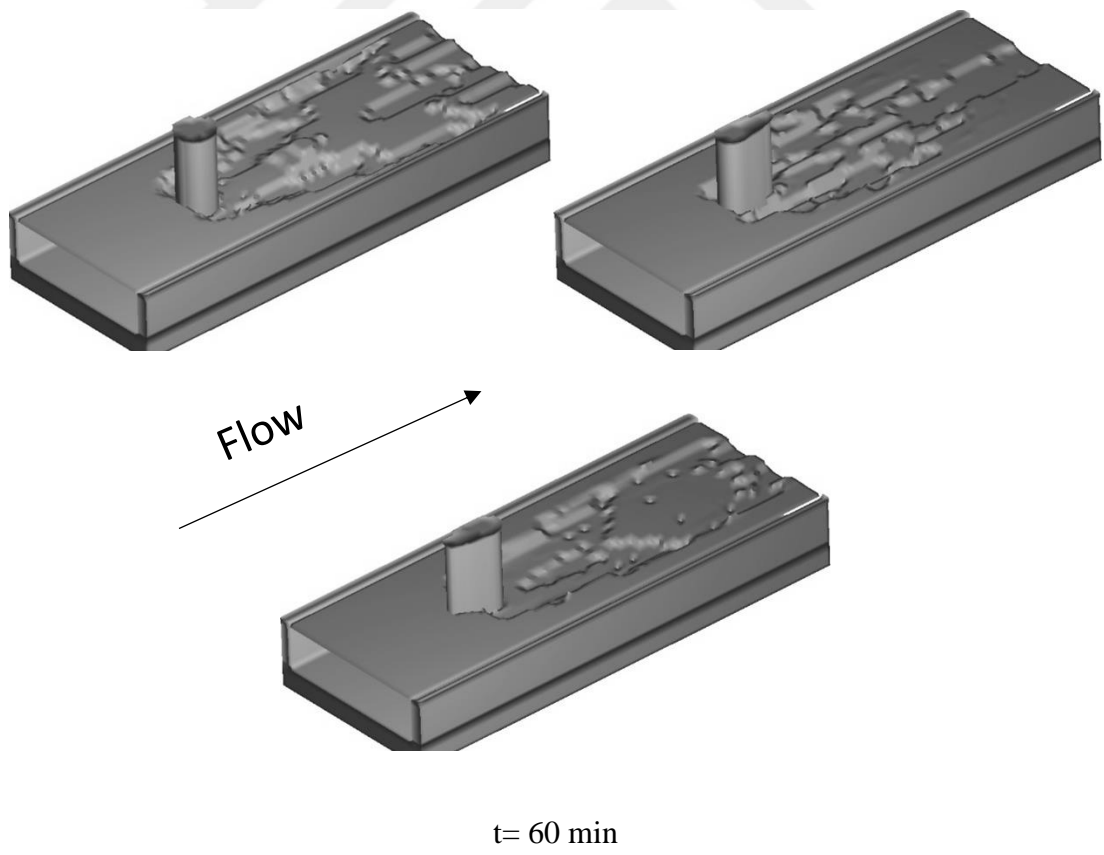
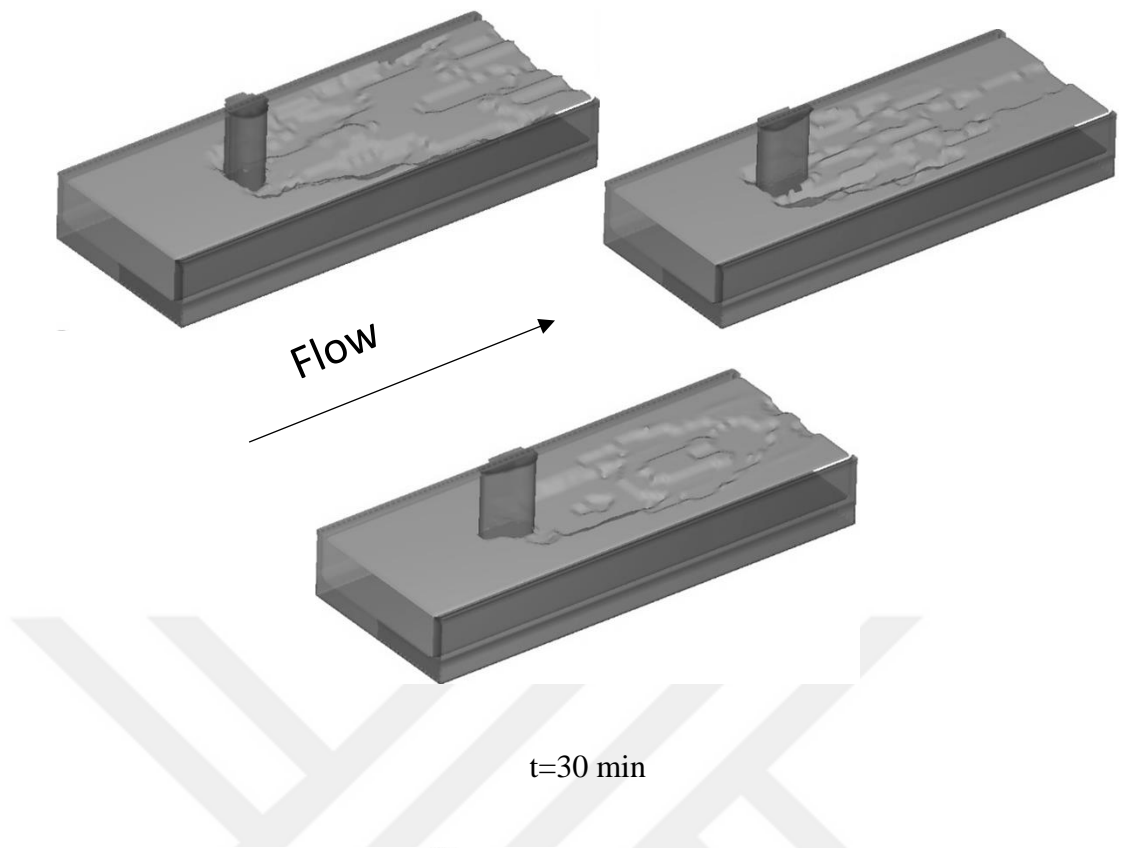
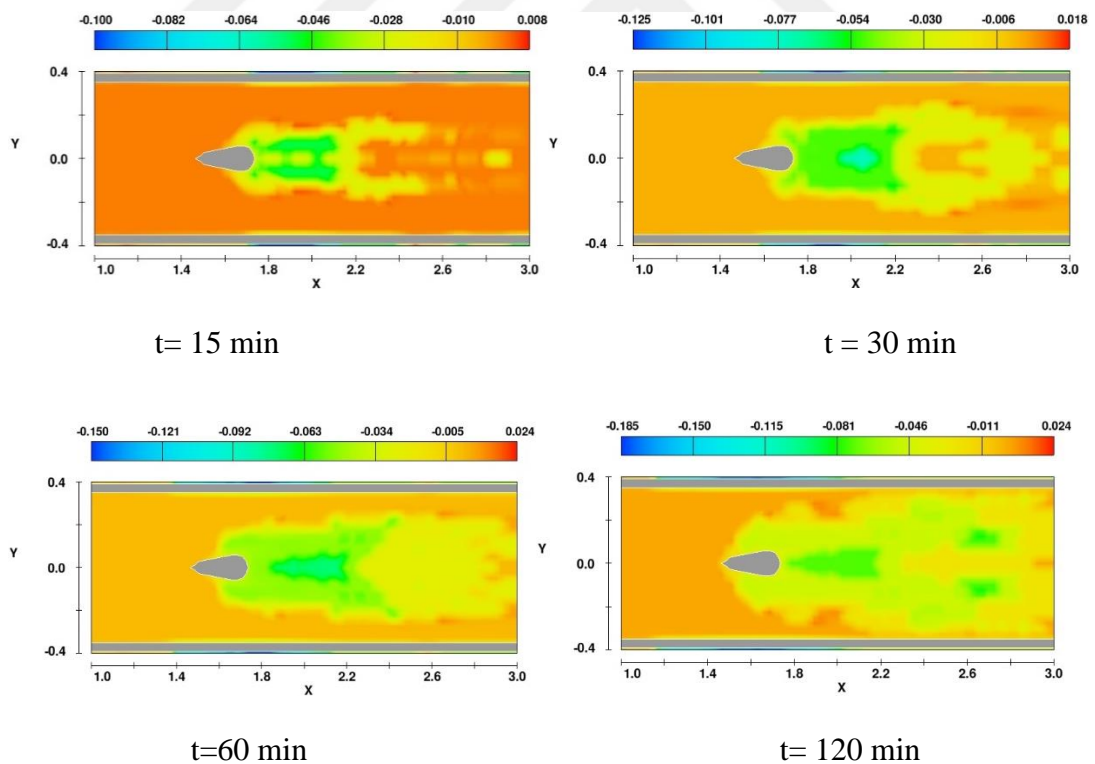
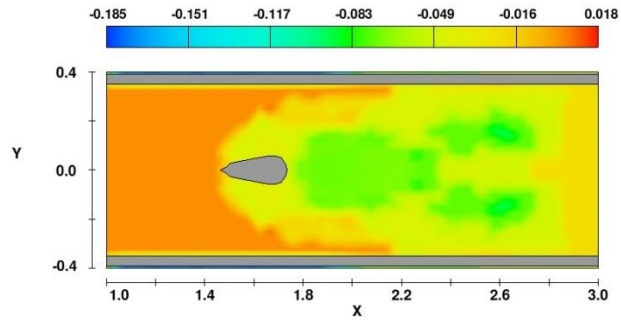


Figure 4.4 3D Plots of scour holes around the all the models at different time.

Figure 4.5 shows the net change of the interface elevation for the circular pier, where the negative and positive values characterize scour depth and deposition height, correspondingly.

It is realized that a scour hole is shaped at two lateral sides of the pier, and there is slight scour closely behind it. This is because the flow around a cylinder is enhanced under the favourable pressure gradient after it passes the cylinder's front nose, which effects in high bed shear stress in the local section. Directly behind the cylinder, the flow has passed the separation points with its direction inverted and speed reduced due to the opposing pressure gradient, causes in bed shear stress lesser than the critical shear stress of flow.



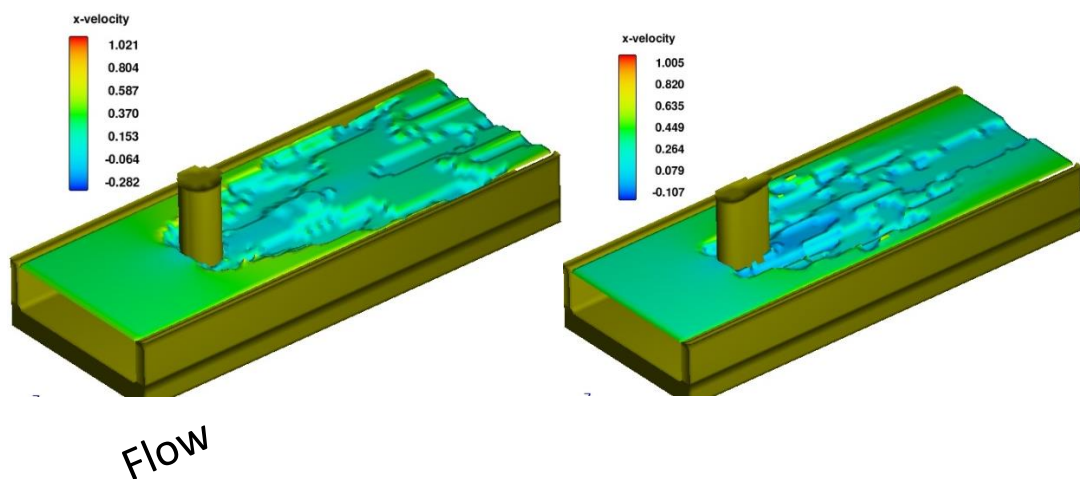


t= 180 min

Figure 4.5 Depth of scour (in negative value) and height of sediment deposition (in positive value) at different time.

4.5 Scour hole versus velocity profiles

Velocity is lowest in the scour hole and increases in the direction of the water interface with soil. Inside the scouring hole Figure 4.6, stream-wise velocity declines with scour depth, eventually reaching negative values. This is revealing of flow reversal that happens because of the horseshoe vortex that is situated in the maximum scour hole. Shen et al. (1969) stated that the flow horseshoe vortex and down-flow increase with pier size. A more flow down the face of the pier to the riverbed can cause greater scour around the pier base. Under the simulated model circumstances, that acts as an open channel, approaching flow velocity meets the pier face and flows downward to the channel bed or upward to form a bow wave.



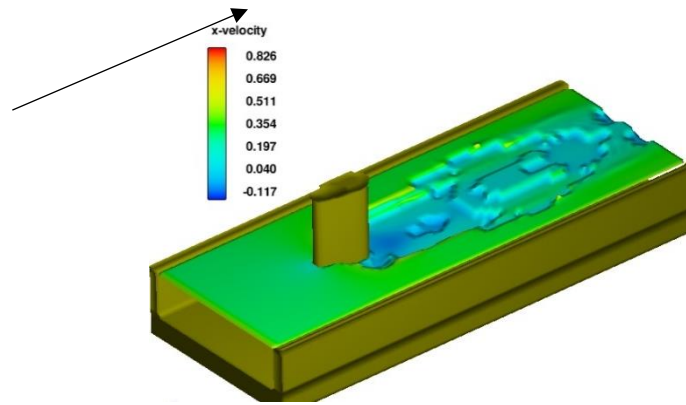


Figure 4.6 Scour hole versus velocity profiles

4.6 Correlation of scour depth versus the Froude number

Aziz (1983) held one of the initial studies to report the positive relationship between Froude number and scour depth. Aziz found that both flow depth and velocity effect pier scour and with increasing Froude number pier scour increased. Wu et al. (2014) similarly notarized that under ice cover condition and open channel flow the Froude number increased with abutment scour depth. The Froude number, U/\sqrt{gH} , indicates the ratio of fluid inertial forces to fluid gravitational forces. A higher Froude number, means a larger resistance exerted by water stream on the river bed material Figure 4.7. In engineering practice, it is standard to link pier scour to flow velocity, flow depth, pier size and also the Froude number (Molinas, 2003).

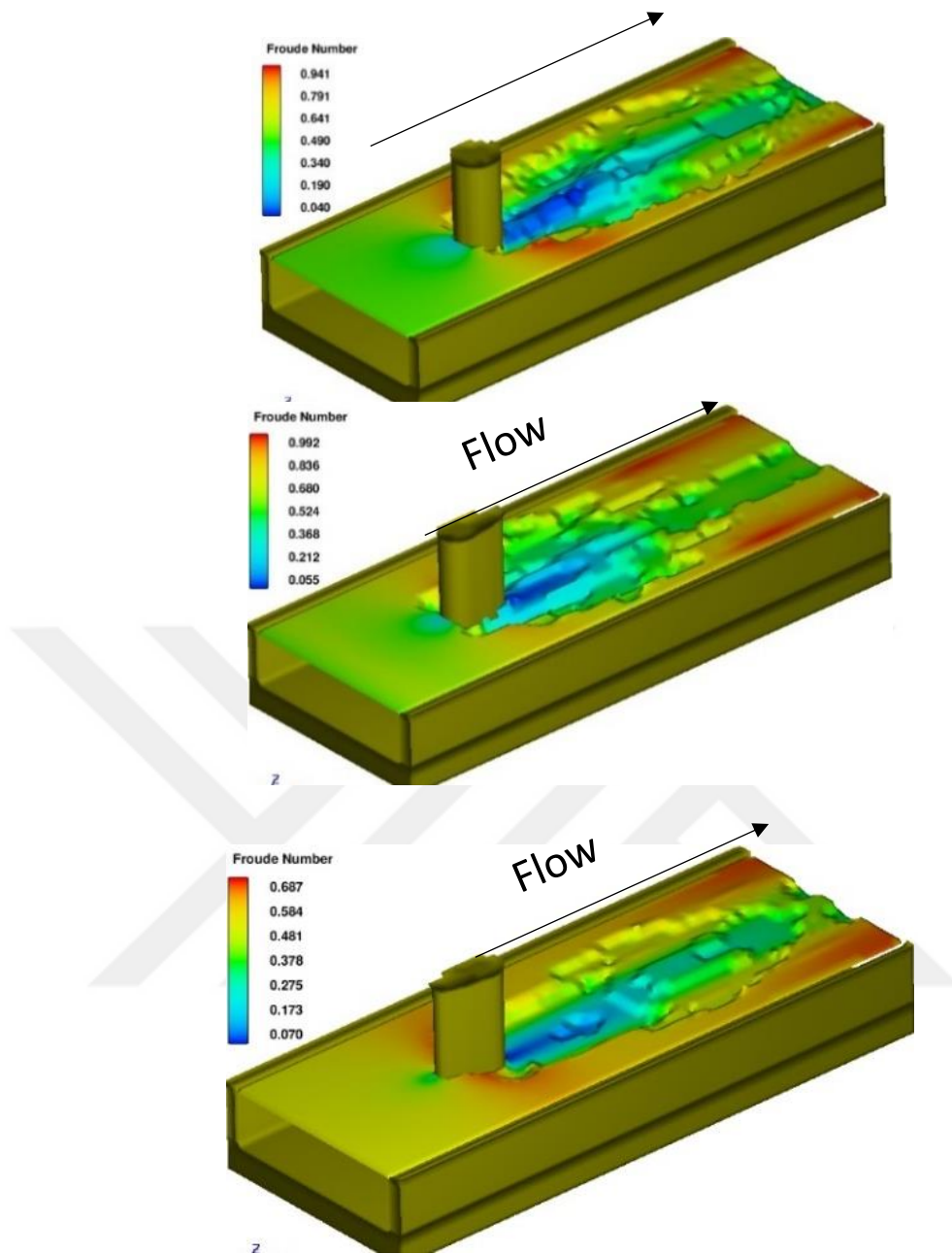


Figure 4.7 Correlation of Froude number versus the scour depth

Of note, however, as pointed out by Melville and Coleman (2000) it is important to notice that the Froude number considered in experimental study might be larger than that for similar field circumstances. While the prototype sediment is smaller than the flume sediment relative to pier size, the flow velocity needed for incipient motion might be greater than the velocity calculated from Froude scaling of prototype flow (Melville and Coleman, 2000). As such, the Froude number considered in flume

experimentations might be bigger than that for the field study, which leads to overestimation of pier scour.

4.6 Velocity vector distribution and their effect

From Fig. 4.8, the effect of different vortices (horseshoe vortex and wake vortex) was detected. At the upstream side of US-FRNP and circular pier geometries, a formation horseshoe vortex was noticed, located at the base of piers. while, for DS-FRNP the influence of the horseshoe vortex minimized because of the down flow being deviate away from the base pier structure. Figure 4.8 shows strong wake vortex and causes scour hole in the awaken section of the piers.

4.7 Scour depth versus turbulent intensity

As the near bed velocity decrease, the kinetic energy applied to the bed also decreases which can have inferences for sediment transport hence why it is being discussed here. Clifford and French (1993) stated that the turbulent kinetic energy specifies the energy that is pulled out from turbulent eddies and is expressed as:

$$\text{TKE} = 0.5(\text{RMS}_x^2 + \text{RMS}_y^2 + \text{RMS}_z^2) \quad (4.1)$$

Practically the turbulence intensity values can be calculated from the standard deviation of (RMS or root mean square) instantaneous velocity fluctuations. The RMS values can be determined based upon the velocity profiles measured in the flume approach flow section.

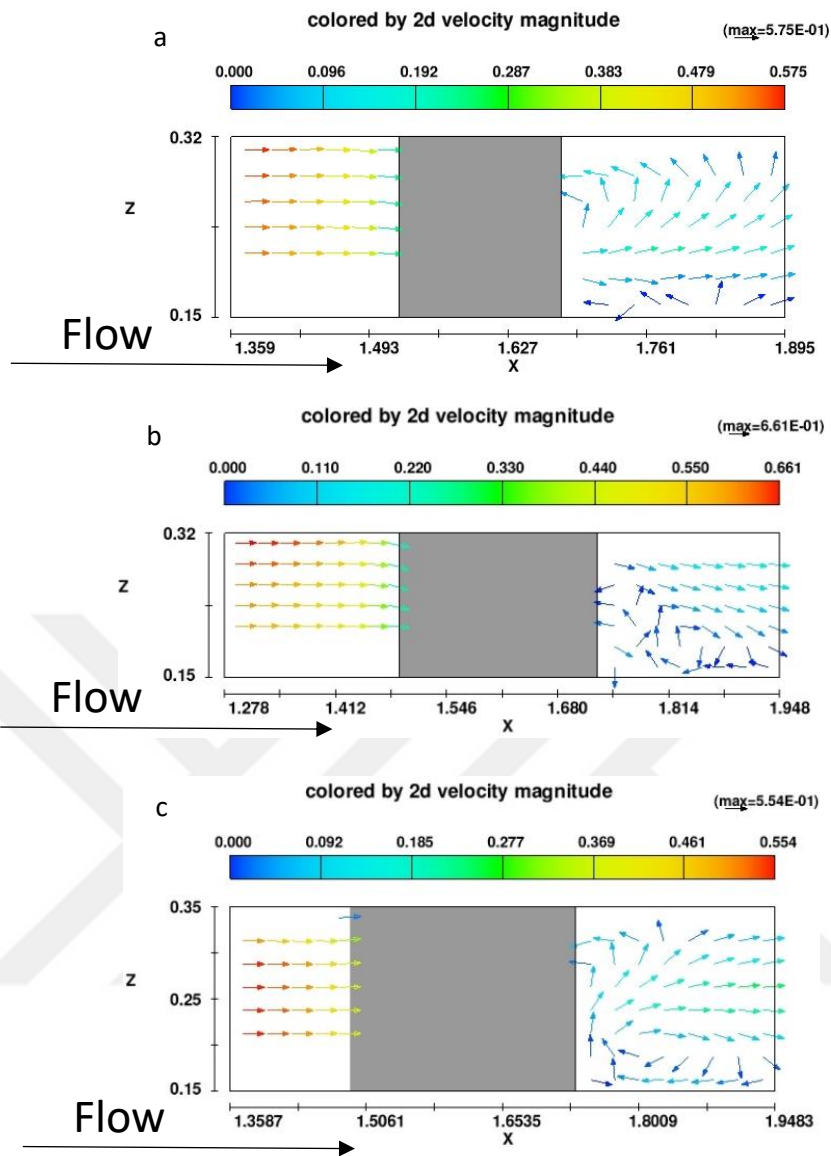


Figure 4.8 Velocity vectors at vertical plane

a circular pier, **b** upstream facing round-nosed pier and **c** downstream facing round-nosed pier

Figure 4.9. shows the 3D turbulent intensity at the same time is a maximum just above the channel bed and produced scour for all conditions. Muste et al. (2000) propose that this is because of the increased turbulence of sediment movement close to the bed. The turbulent intensity decreases at other places of the model. Also, the turbulent kinetic energy behind the pier is isotropic and stronger than the turbulence upstream of the cylinder (Graf and Istiarto, 2002).

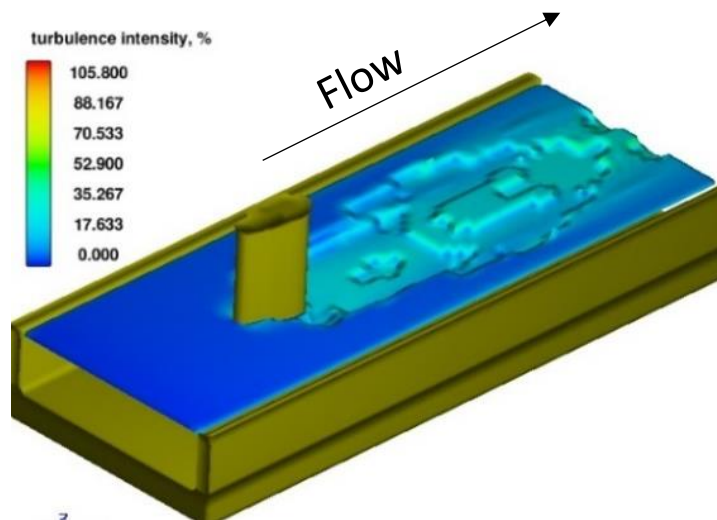
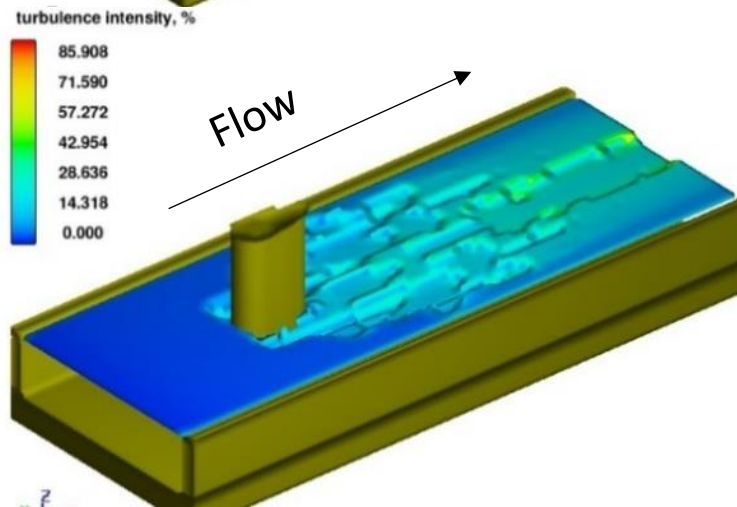
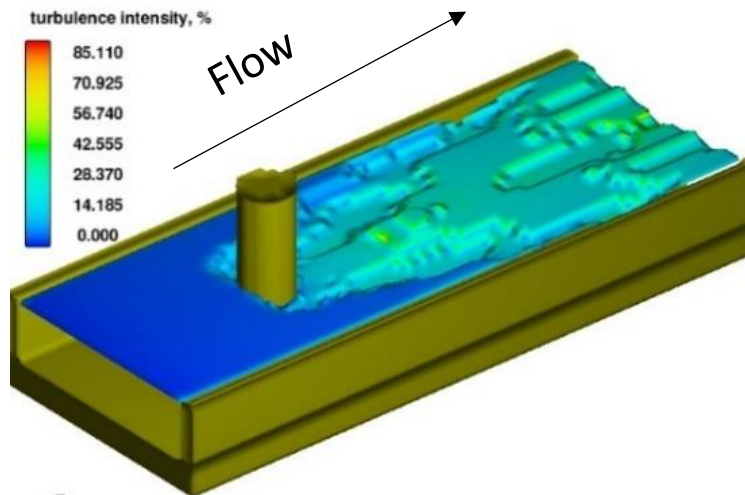


Figure 4.9 Scour depth versus turbulent intensity

CHAPTER 5

CONCLUSIONS AND RECOMMENDATIONS

5.1 CONCLUSION

The role of this research to the phenomenon of bridge pier scour calculation depends on mainly in the development of an improved bridge pier shape for scouring reduction that is based not only on the general experimental study but also on complete CFD Modelling used for scour prediction. Additionally, the proposed bridge pier shape and geometry technique developed in the experimental study also found to have the same outcome in this investigation and the conclusions are strongly built on comparisons with experimental results. The study has an important application in designing bridge geometry in real-world cases so that scour can be reduced significantly.

Most important results and conclusions from the study are presented below.

- The ability of the Flow-3D program has been confirmed by simulating existing experimental study and comparing the numeric results with experiment outcomes.
- The Flow-3D results from this study, when combined with experimental data from the literature, have led to a modified Bridge pier shape that describes the same effect of pier shape on scouring reduction.

- This study presents good agreement between experiment and numerical results for scour depth and velocity distribution the only position of maximum depth of scour is not occurred at the same location,



as the maximum scour hole depth was located in the nose of the piers in the experimental study. But, in the numerical study, the holes formed at lateral sides near the downstream face of the bridge pier and this can be due to the weak horseshoe vortex that formed in the nose of the pier in the numerical model. According to Laursen and Toch (1956) when we have weak horseshoe vortex in the system, location of maximum depths of scour moves towards the downstream end of the pier.

- The results of comparison between the both studies reveal that DS-FRNP when related to the other models is an effective countermeasure to decrease depth of scour as it reduces depth of scour, scour hole length and width as.
- The results from both studies showed that placing round-nosed bridge pier downstream facing to the flow lead to improvement in its performance significantly.
- Flow-3D is a powerful tool to complement experimental investigation. But, extensive term simulations have to be made to validate the model's ability accurate scouring analysis. Specific consideration has to be paid on the mesh resolution and turbulence model features that may affect the results.

5.2 Recommendation

In general, the phenomenon of scour process at a bridge pier are studied widely through field monitoring and by experimental and numerical approaches. Still, the interaction between local scour which is mainly affected by the geometry of the, should be studied in more detail. Using physical river modeling with river bathymetry constructed following the design geometry obtained in this study, more precise and practical calculations for total scour depth can be expected.

The results of this investigation could be advanced by the engineers and designers, which can be practiced in real world design.

Bridge sites experience successive numerous flood events during the rainy season and scouring frequently occurs under live-bed scour conditions which scour holes' refills after the flood has passed especially during smaller floods. Which is not well understood and need more attention and consideration in the future studies.



REFERENCES

Abbot, M. and Basco, D. (1989). Computational fluid dynamics: An introduction for Engineers.

Adnan, I., Mustafa, G. and Hamid, H. H., (2015). Effect of Bridge Pier Position on Scour Reduction According to Flow Direction, *Arab J. Sci. Eng.*, **40**:1579–1590.

Afzal, M. A., Bihs, H., A. Kamath and Arntsen, Q. A., (2014). Three dimensional numerical modelling of pier scour under current and waves using level set method, in: *Proc. 33rd International conference on Ocean, Offshore and Arctic Engineering, Volume 2: CFD and VIV, San Francisco, USA, 2014.*

Alabi, P. (2006). Time development of local scour at a bridge pier fitted with a collar. *MSc Thesis. University of Saskatchewan, Saskatoon, Saskatchewan.*

Andrey, B. and Gareth, P. (2000). Flume study of the effect of relative depth on the incipient motion of coarse uniform sediments, *Journal of Water Resources Research*, **36 (2)**, 619-628.

Anu, A. and Jennifer, G. D., (2011). experimental study and numerical simulation of flow and sediment transport around a series of spur dikes” *PhD thesis, university of Arizona, Arizona, USA.*

Ataie-Ashtiani, B. and Beheshti, A. A. (2006). “Experimental investigation of clearwater local scour at pile groups”. *J. Hyd. Eng., ASCE*, **132 (10)**, 1100-1104.

Aziz, I. (1983). Dimensional analysis as applied to scouring around bridge piers in alluvial rivers. *Jurnal Teknologi Billiten*, **3**, 59-66.

Beheshti, A. and Ataie, B. (2008). Analysis of threshold and incipient conditions for sediment movement. *Journal of Coastal Engineering*, **55**, 423-430.

- Brethour, j., (2003). Modeling Sediment Scour. Flow Science, Inc. Report FSI-03-TN62.
- Breusers, H., Nicollet, G. and Shen, H. (1977). Local scour around cylindrical piers. *Journal of Hydraulic Resources*, **15 (3)**, 211-252.
- Buffington, J. and Montgomery, D. (1997). A systematic analysis of eight decades of incipient motion studies, with special reference to gravel-bedded rivers. *Water Resources Research*, **33 (8)**, 1993-2029.
- Chabert, J. And P. Engeldinger, (1956). Scouring around piles of bridges; Lab. Nat. Of Hydr. *Chatou*, October.
- Chang, H. (1992). Fluvial Processes in River Engineering. *Krieger Publishing Company, Florida*, 432p.
- Chiew, Y. M., (1992), Scour protection at bridge piers, *Journal of Hydraulic Engineering, ASCE*, **Vol. 118, No. 11**, pp. 1260–1269.
- Chiew, Y. M., and Lim F. H. (2000). Failure behavior of riprap layer at bridge piers under live-bed conditions. *Journal Hydraulic Engineering, ASCE*, **Vol. 126, No. 1**, pp. 43–55.
- Clifford, N. and French, J. (1993). Monitoring and modelling turbulent flows: historical and contemporary perspectives. In *Turbulence: Perspectives on flow and sediment transport*, (Eds. Clifford N., French, J., and Hardistry, J). *Wiley: Chichester*, 1-34.
- Dey, S. and Rajkumar V. R., (2007). Clear-water scour at piers in sand beds with an armor layer of gravels. *Journal of Hydraulic Engineering, ASCE*, **Vol. 133, No. 6**, pp. 703–711.
- Diab, R., Zanke, U. and Link, O., (2010). 3D turbulent flow field at square pier in a gravel scour hole. *International Conference on Fluvial Hydraulics “River Flow 2010” Braunschweig*, 691-697.

Escarameia, M., (1998). Laboratory investigation of scour around large structures in tidal waters. *Conf. Basics of Sediment Transport and Scouring*. HR Wallingford.

Ettema, R., (1980). Scour at Bridge Piers. *University of Auckland, School of Engineering, Auckland, New Zealand*, Rep. **No. 216**.

Froehlich, David C., (1989). "Local scour at bridge abutments.", *Proc. National Conference of Hydraulic Engineering*, ed. M.A. Ports, ASCE, New Orleans, LU, pp.13-18

Flow Science, Inc., (2009). FLOW-3D user's manual, 9.4 edition, *Flow Science, Inc., Santa Fe*.

Graf, W. and Istiarto, W. (2002). Flow pattern in the scour hole around a cylinder. *Journal of Hydraulic Research*, **40 (1)**, 13-20.

Gupta, A. K. and Gangadharaiyah T., (1992). Local scour reduction by a delta wing-like passive device. Proceeding, *8th Congr. of Asia and Pacific Reg. Div., 2, CWPRS, Pune, India*, B471–B481.

Habert, J. and Engeldinger P., (1956). Study of scour around bridge piers; *Lab. Nat. of Hydr. Chatou*.

Hirt, C. W., and Nichols, B. D., (1981). "Volume of fluid (VOF) method for the dynamics of free boundaries." *J. Comp. Phys.*, **39**, 201-225.

Kanellopoulos, P., (1998). Incipient motion under shallow flow conditions. *MSc Thesis. Virginia Polytechnic Institute and State University, Blacksburg, Virginia*.

Kummar V., Ranga Raju K. G. and Vittal N., (1999). Reduction of local scour around bridge piers using slot and collar. *Journal of Hydraulic Engineering*, **Vol. 125, No. 12**, pp. 1302–1305.

Lagasse, P., Zevenbergen, L., Schall, J. and Clopper, P., (2001). Bridge scour and stream instability countermeasures: Experience, selection, and design guidelines. FHWA NHI 01-003: Federal Highway Administration, Hydraulic Engineering Circular No. 23, 2nd ed., *U.S. Department of Transportation, Washington, D.C*

Laursen, E. M. and A. Toch, (1956). Scour around bridge piers and abutments; Bull. No. 4, *Iowa Highway Res.Board*.

Laursene , M., (1960). Scour at bridge crossings; *Proc. ASCE*, **86**, (HY 2), pp. 39/54 (also 1962, Trans. ASCE, **127 (I)**, p. 166/209).

Lauder, B. E. and Spaulding, D. B., (1972). Mathematical models of turbulence. Academic Press, *New York, N.Y.*

Liu , X., Garcia , M., (2008). Three-dimensional numerical model with free water surface and mesh deformation for local sediment scour, *Journal of Waterway, Port, Coastal and Ocean Engineering* **134**, 203–217.

Manouchehr H., Hossein A. and Elham I., (2010). Reduction of local scour around bridge pier groups using collars, *International Journal of Sediment Research*, **Vol. 25, No. 4**, pp. 411–422.

Margheritini, L., Martinelli, L., Lamberti, A. and Frigaard, P., (2006). Erosion caused by waves and tidal currents around large diameter piles. *XXX Conference of Hydraulics and Hydraulic Construzioni, Rome*.

May, R.W.P. and Escarameia, M., (2002). Local scour around structures in tidal flows. *First International Conference on Scour Foundations, Texas A&M University*.

Melville, B.W., Chiew, Y.M., (1999). Time scale for local scour at bridge piers. *J. Hydraul. Eng. ASCE* **125 (1)**, 59–65.

Melville, B. and Coleman, S., (2000). Bridge Scour. *Water Resources Publications, LLC, Highlands Ranch, Colorado, USA*.

Moody, J. A., Smith, J. D. and Ragan, B. W., (2005). Critical shear stress for erosion of cohesive soils subjected to temperatures typical of wildfires, *Journal of Geophysical Research: Earth Surface*, 110 (F1).

Mostafa, E., (1994). Scour around skewed bridge piers. *PhD Dissertation. Alexandria University, Alexandria, Egypt*.

Molinas, A., (2003). Bridge scour in non-uniform sediment mixtures and in cohesive materials: synthesis report. Report No. FHWA-RD-03-083, *Federal Highway Administration, McLean, Virginia*.

Muste, M., Braileanu, F. and Ettema, R., (2000). Flow and sediment transport measurements in a simulated ice-covered channel. *Water Resources Research*, **36** (9), 2711-2720.

Muzzammil, M., Gangadharaiah, T. and Gupta, A. K., (2004). An experimental investigation of a horseshoe vortex induced by a bridge pier. *Water Management Journal*, Proceedings of the Institution of Civil Engineers, Thomas Telford Journals, London, **157** (2), 109- 119. Paper 13904.

Nadeem, A., Hans, B., Arun, K. and Oivind A., (2015). Three-dimensional CFD modeling of wave scour around side-by-side and triangular arrangement of piles with REEF3D, *Procedia Engineering*, **116**, 683 – 690.

Niezgoda, Sue L., and Johnson, Peggy A., (1999). Abutment scour at small severely contracted bridges. Proc., Cold Regions Engineering 'Putting Into Practice', ASCE, Lincoln, NH, pp.600-611.

Odgaard, A. J. and Wang, Y., (1987). Scour prevention at bridge piers. *Hydr. Engrg.* '87, R. M. Ragan, ed., *National Conference, Virginia*, pp. 523–527.

Olsen, N. R. B. and Melaan, M. C., (1993). "Three-dimensional calculation of scour around cylinders". *J. Hyd. Eng., ASCE*, **119** (9),1048-1054.

Olsen, N. R. B., Kjellesvig, H. M., (1998). Three-dimensional numerical flow modelling for estimation of maximum local scour depth, *IAHR Journal of Hydraulic Research* **36**, 579–590.

Ozalp, M. (2013). Experimental investigation of local scour around bridge pier groups. *MSc Thesis. Middle East Technical University, Cankaya Ankara, Turkey*.

Pitt, R., Clark, S. E. and Lake, D., (2007). *Construction site erosion and sediment controls - Planning, design and performance*, DEStech Publications, Inc.

Paintai, A. S. and Garde, R. J., (1965). Effect of inclination and shape of obstruction on local scour; *Res. Journal, Univ. of Roorkee, Uttar Pradesh, India*. **Vol. 8**.

Raudkivi, A.J. and Ettema, R., (1983). Clear-water scour at cylindrical piers. *Journal of Hydraulic Engineering*, **109 (3)**, 339-350.

Rehbock, Th., (1921). Transformations wrought in stream beds by bridge piers of various shapes of cross sections and experiments on the scouring action of the circular piers of a skew railroad bridge across the Wiesent River for the Nürnberg Railroad; Hydraulic Laboratory Practice, Joho R. Freeman, ed. *ASME, New York*, 1929.

Richardson, E. and Davies, S., (1995). Evaluating scour at bridges, *FHWA, U.S. Department of Transportation, Washington, D.C.* Rep. No. FHWAIP-90-017 (HEC-18).

Richardson, E. V. and Davis, S. R., (2001). "Evaluating scour at bridges, Fourth edition", Hydraulic engineering circular **No.18**, p380, *Federal Highway Administration, U.S. Department of Transportation Report No. FHWA NHI 01-001 HEC-18*.

Robert, E., Tatsuaki, N., and Marian M., (2006). an illustrated guide for monitoring and protecting bridge waterways against scour, *Iowa Highway Research Board, Project TR-515 Final Report, IIHR Technical Report No. 449*.

Rodi, W., (1980). Turbulence models and their application in hydraulics: A state of the art Review. *IAHR*.

Romita, P. L., (1960), Discussion on Laursen (1960). *Proc. ASCE*, **86, HY9**, pp. 151/152.

Roulund, A., Sumer, B. M., Fredsoe, J. and Michelsen, J., (2005). "Numerical and experimental investigation of flow and scour around a circular pile". *J. Fluid Mechanics*, **534**, 351-401.

Shaw, C. T., (1992). Using computational fluid dynamics. *Prentice Hall, New York, N.Y.*

Shields, A., (1936). Application of similarity principles and turbulence research to bed-load movement. Trans., W.P. Ott and J.C. van Uchelen. *California Institute of Technology, Pasadena: USDA, Soil Conservation Service Cooperative Laboratory, Hydrodynamics Laboratory, Publ. No. 167*

Shen, H. and Schneider, V., (1969). Local scour around bridge piers. *Journal of the Hydraulics Division, Proceedings of the American Society of Civil Engineers, 95 (6)*, 1919-1941.

Shen, H. W. and Schneider, V. R., (1970). Effect of bridge pier shape on local scour; Prepr, *ASCE Nat. Meeting on Transport Eng., Boston, Mass., No. 1238*.

Sturm, T.W., (1999). Abutment scour in compound channels, In *Stream Stability and Scour at Highway Bridges*, ed. E. V. Richardson and P.F. Lagasse, *ASCE*, pp. 443-456.

Sumer, B. M., Fredsoe, J., (2001). Scour around pile in combined waves and current, *Journal of Hydraulic Engineering 127*.

Tison, L. J., (1961). Local scour in rivers; *J. Geoph. Res.*, **66 (12)**, p. 4227/4232.

Tulimilli, B. R., Majumdar, P. and KOSTIC M., (2003). Development of CFD Simulation for 3-D Flooding Flow and Scouring Around a Bridge Structure, *Argonne National Laboratory West Chicago, IL U.S.A*

UNEP, (2000). Guidelines for erosion and desertification control management, *United Nations Environment Program (UNEP) and Food and Agriculture Organization (FAO)*.

Varzeliotis, A. N., (1960). Model studies of scour around bridge piers; M.Sc. Thesis Dept. of Civil Eng., *Univ. of Alberta*.

Vasquez, J. A., Walsh, B. W., (2009). CFD simulation of local scour in complex piers under tidal flow, *33rd International Association of Hydraulic Engineering & Research (IAHR) Congress: Water Engineering for a Sustainable Environment*.

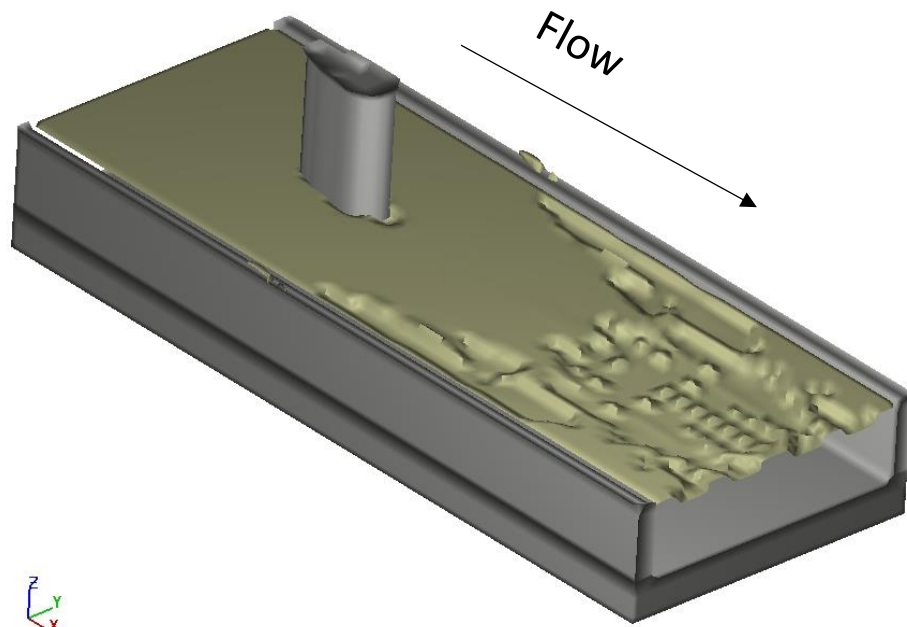
- Vollmer, A. and Kleinhans, M., (2007). Predicting incipient motion, including the effect of turbulent pressure fluctuations in the bed. *Water Resources Research*, **43**, 1-16.
- Wu, S. and Rajaratnam, N., (1996). Transition from Hydraulic Jump to Open Channel Flow, *Journal of Hydraulic Engineering*, **122 (9)**, 526-528.
- Wu, P., Hirshfield, F., Sui, J., Wang, J., and Chen, P., (2014). Impacts of ice cover on local scour around semi-circular bridge abutment. *Journal of Hydrodynamics*, **26 (1)**, 10-18.
- Xu, P. and Yu, B., (2008). “Developing a New Form of Permeability and Kozeny-Carman Constant for Homogeneous Porous Media by Means of Fractal Geometry”. *Advances in Water Resources*, **31**, 74-81.
- Yanmaz, A. M., Altinbilek, H. D., (1991). Study of Time-Dependent Local Scour around Bridge Piers, *J. Hydraulic Engineering*. **Vol. 117, No.10**,1247-1268.
- Yanmaz, A., (2002). Dynamic reliability in bridge pier scouring. *Turkish Journal of Engineering and Environmental Sciences*, **26**, 367-375.
- Yarnell, D. L. and Nagler, F. A., (1931), A report upon a hydraulic investigation of North Carolina standard reinforced concrete bridge pier, No. P-401-R and modifications thereof; *Iowa Inst. of Hydr., Res., Univ. of Iowa, Iowa City*.
- Zevenbergen, L., Ameson, L., Hunt, J. and Miller, A., (2012). Hydraulic design of safe bridges. *FHWA-HIF Report 12-018-HDS 7*.
- Zhao, M., Cheng, L. and Zaong, Z., (2010). Experimental and numerical investigation of local scour around a submerged vertical circular cylinder in steady currents. *Coastal Engineering*, **57**, 709-721.



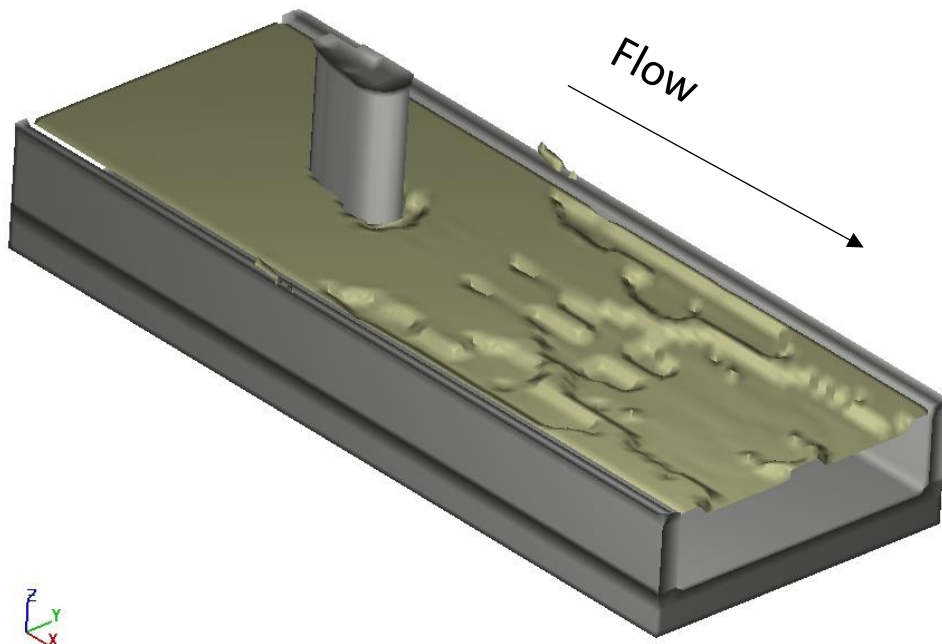
APPENDICES

APPENDIX A

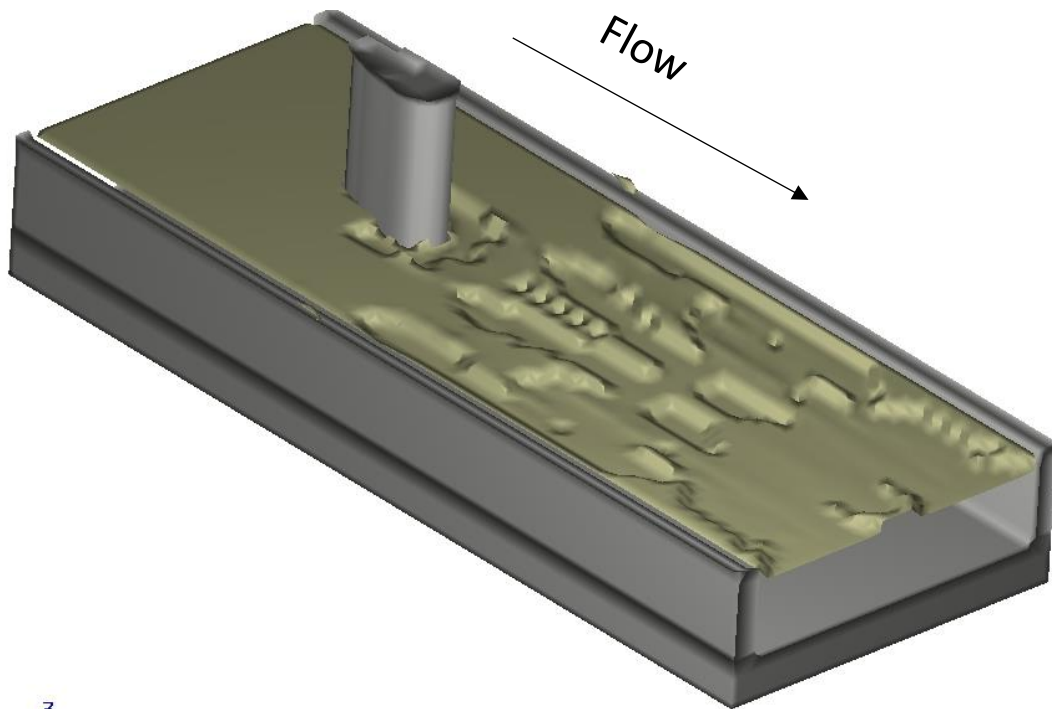
Figures of scour development with time for DS-FRNP at different discharge.



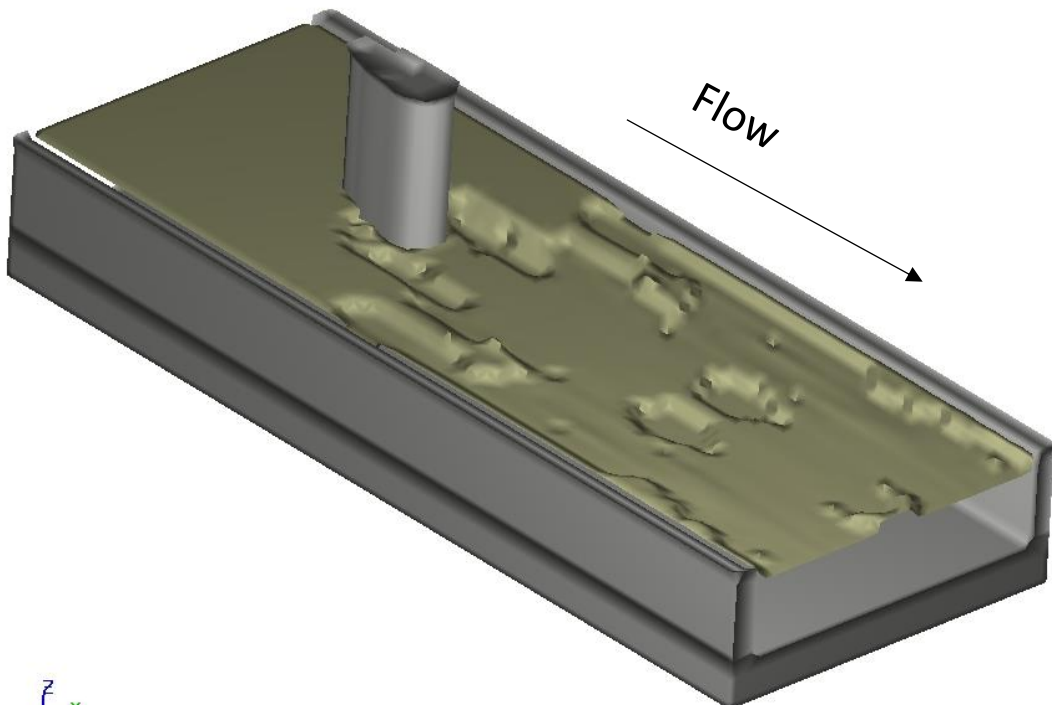
t= 5 min.



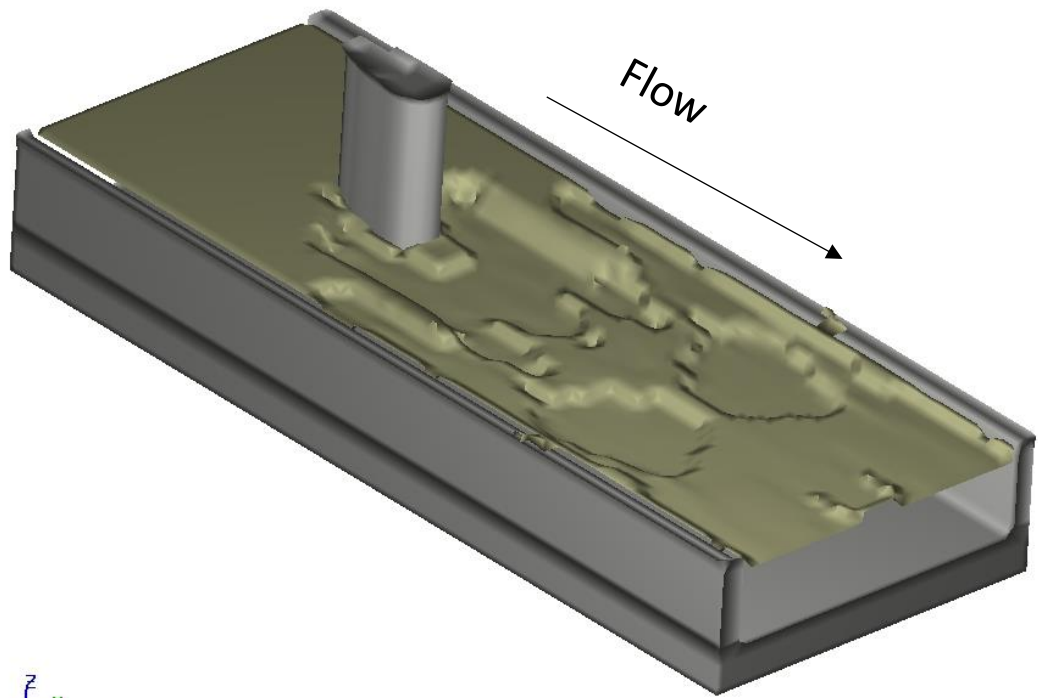
t= 15 min.



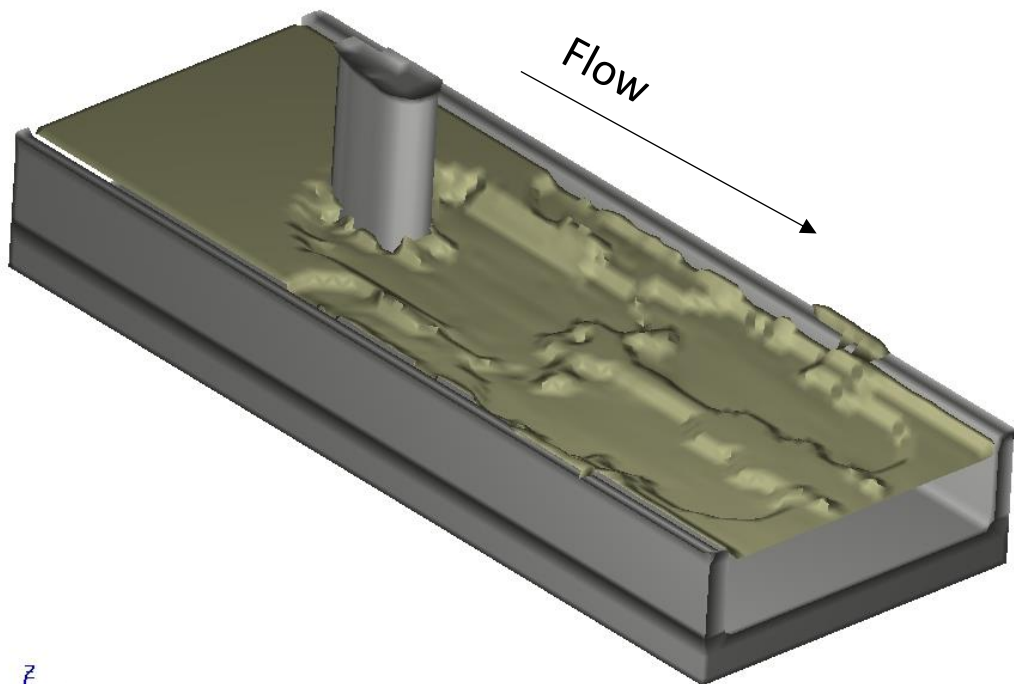
t= 30 min.



t= 60 min.

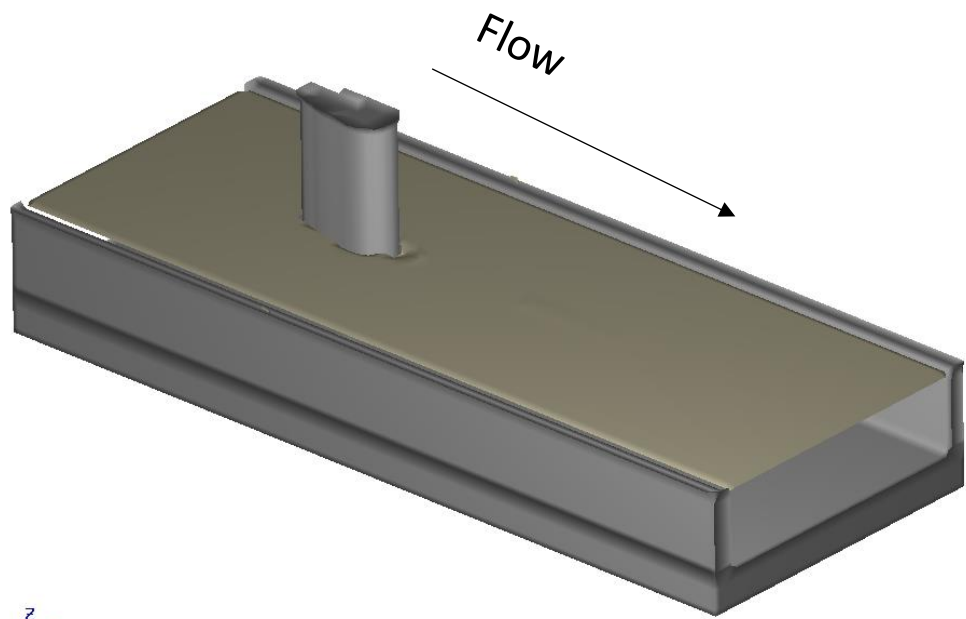


t= 120 min.

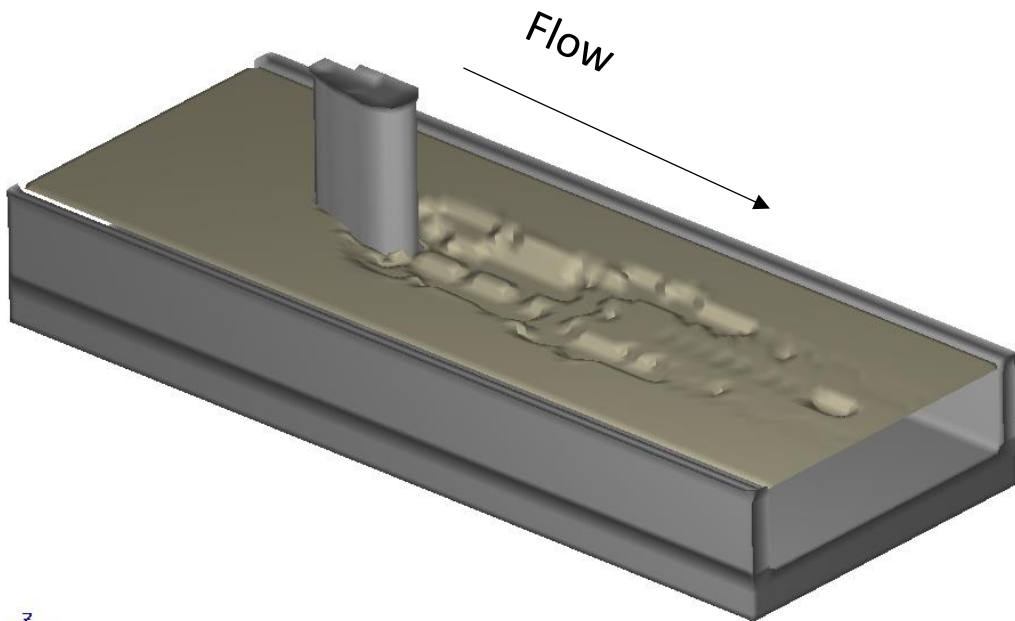


t= 180 min.

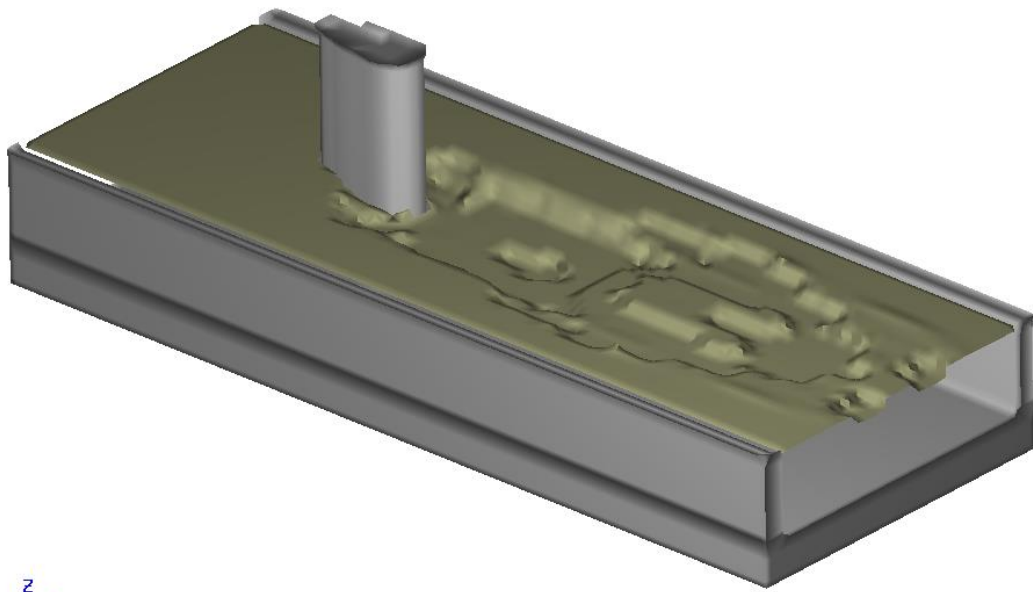
Figure A.1 Scour development versus time $Q=48$ l/s



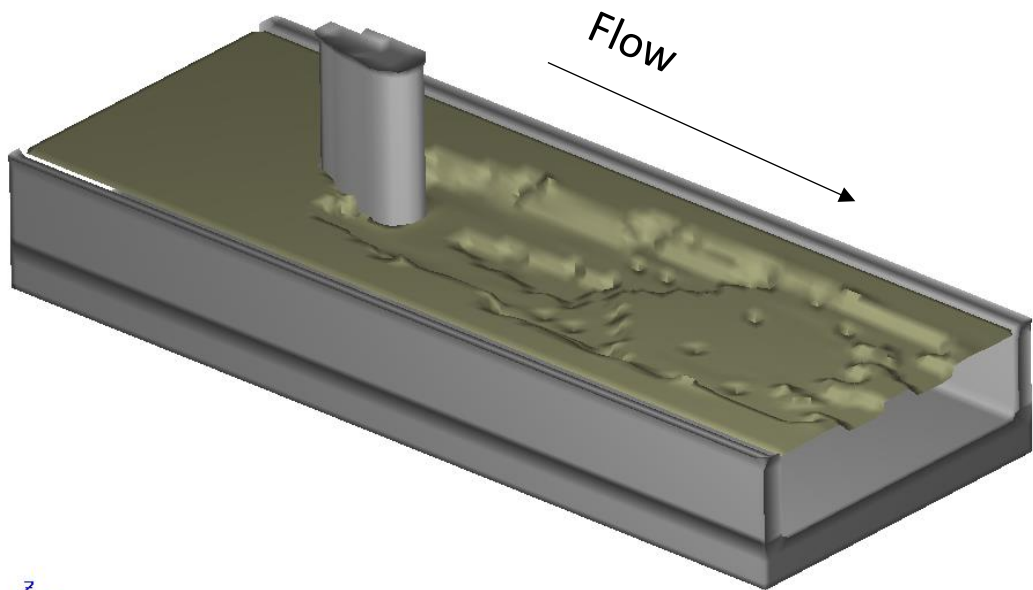
t= 5 min.



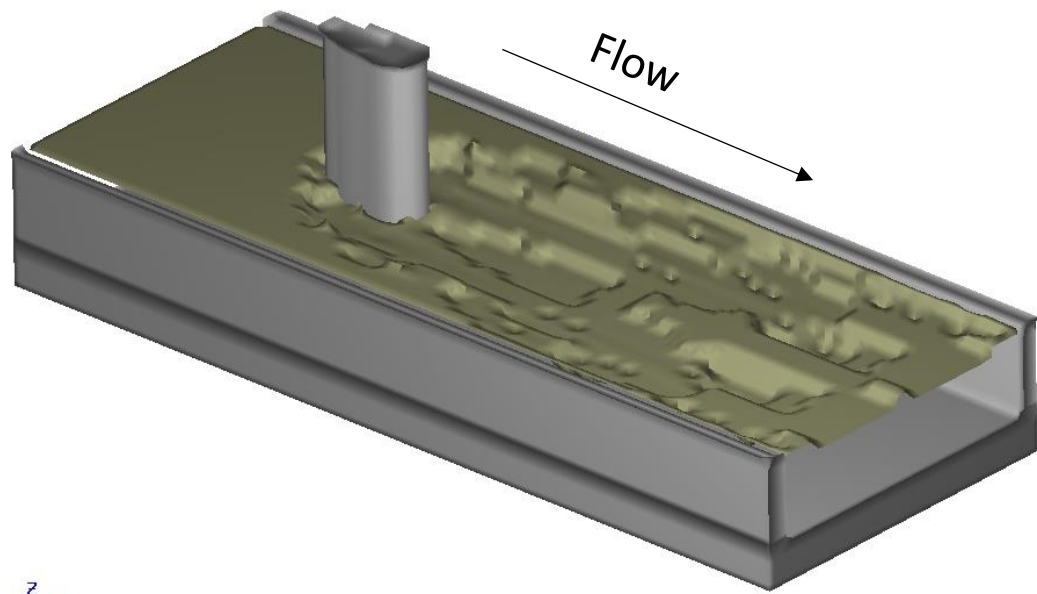
t= 15 min.



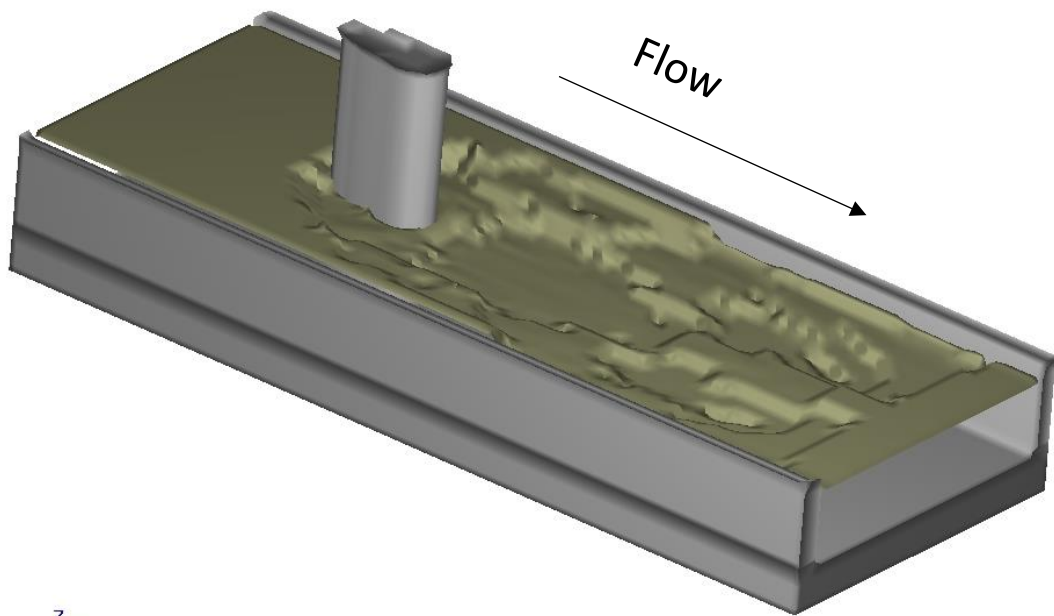
t= 30 min.



t= 60 min.



t= 120 min.



t= 180 min.

Figure A.2 Scour development versus time $Q=58$ l/s

APPENDIX B

Figures of two-dimensional water surface profile at different discharge.

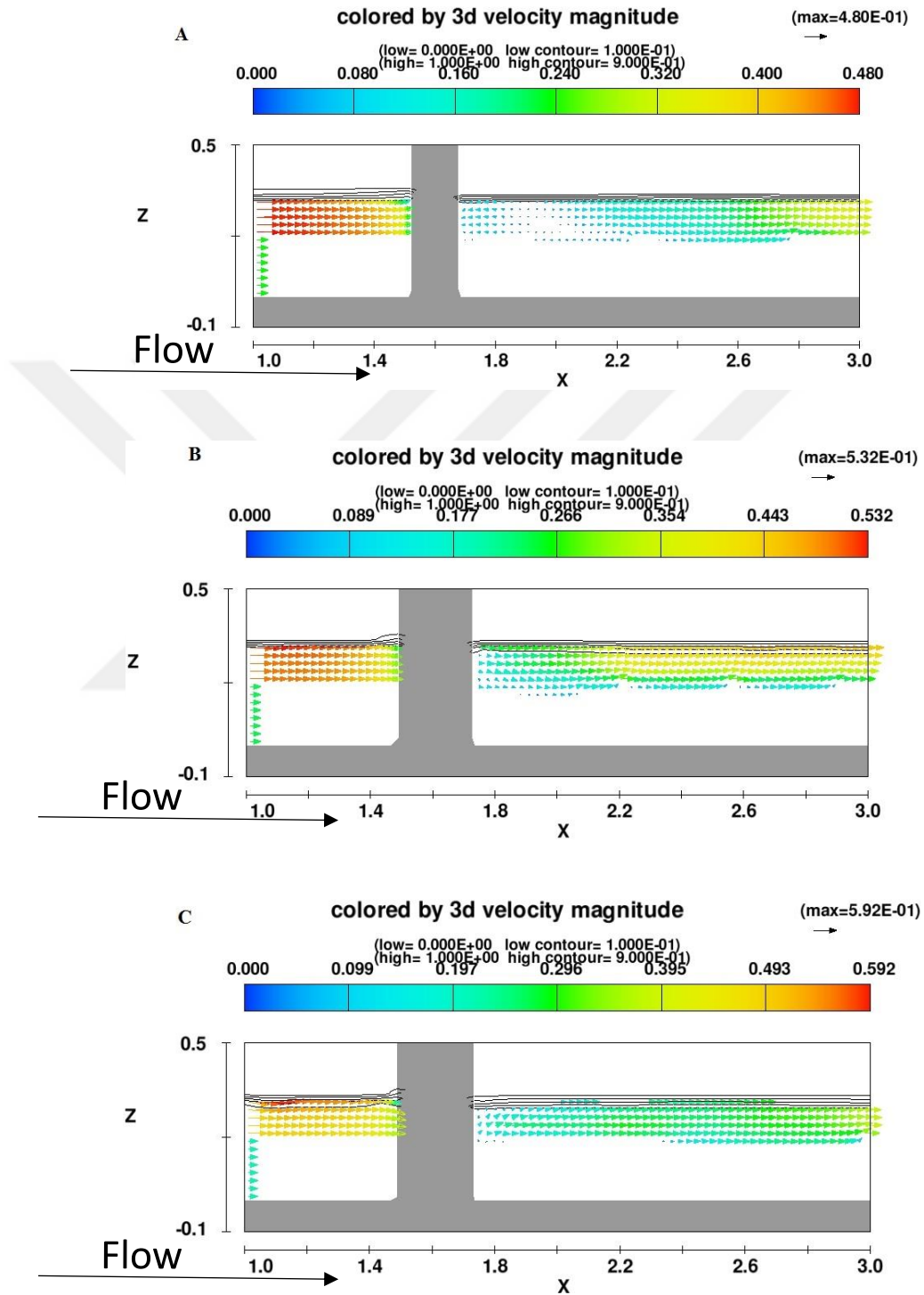


Figure B.1 Two-dimensional water surface profile at t=30 min. and Q=48 l/s,

A-Circular Model, B-US-FRNP, C-DS-FRNP.



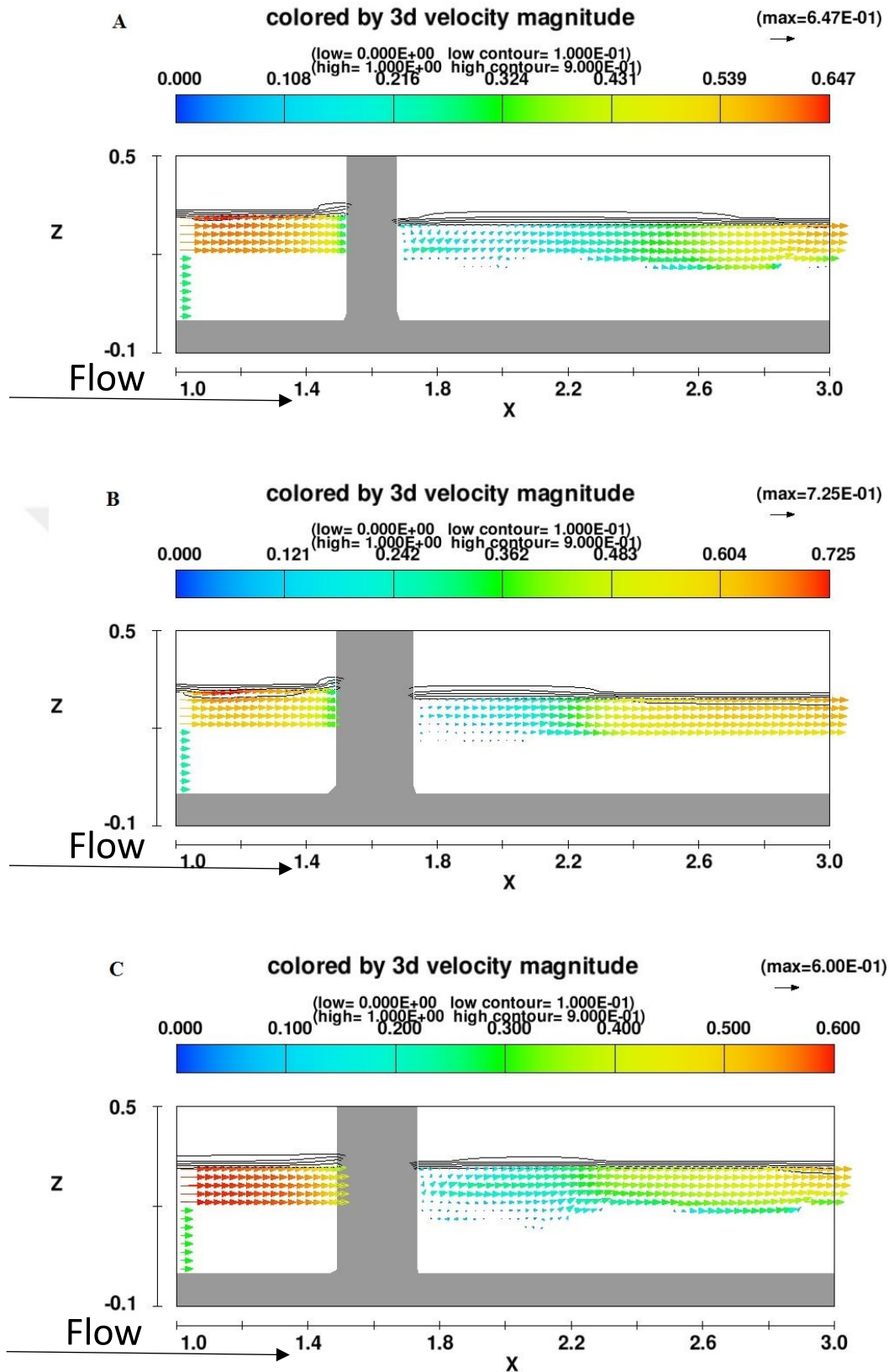


Figure B.2 Two dimensional water surface profile at (t=30 min.) and Q=58 l/s,

A-Circular Model, B-US-FRNP, C-DS-FRNP.

APPENDIX C

Figures of two-dimensional velocity magnitude at different discharge.

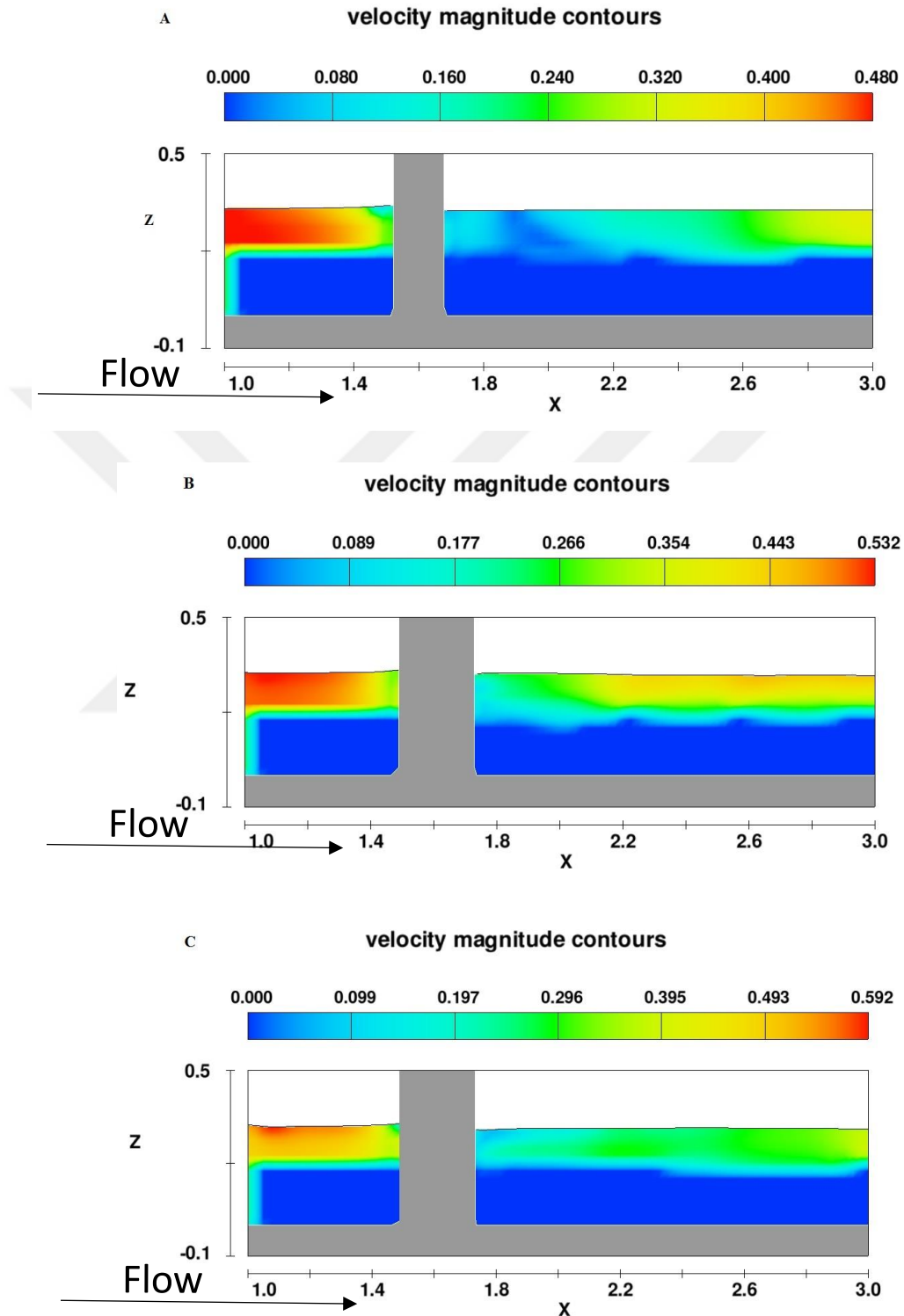


Figure C.1 Two-dimensional velocity magnitude at (t=30 min.) and Q=48 l/s,

A-Circular Model, B-US-FRNP, C-DS-FRNP.

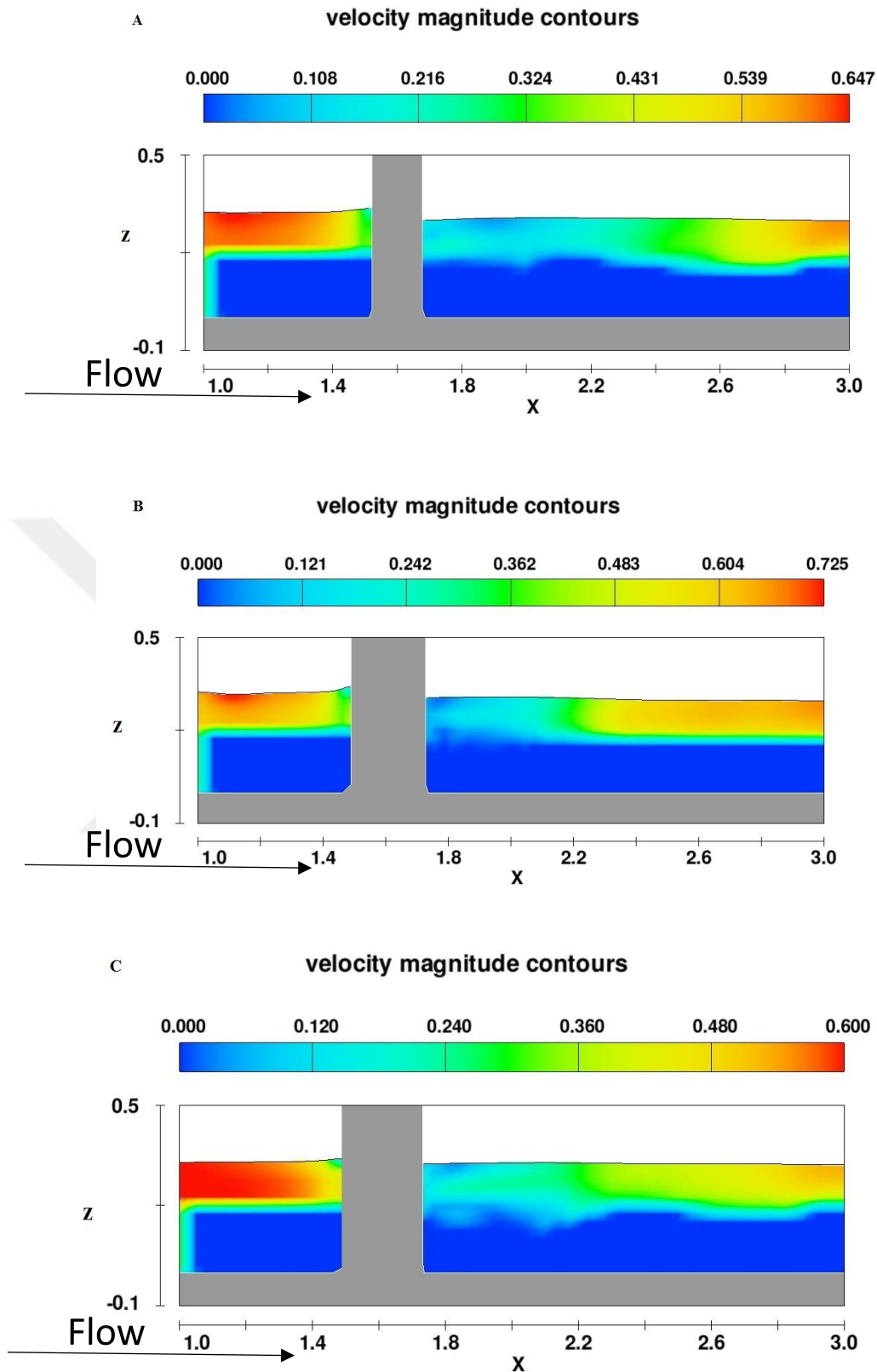


Figure C.2 Two-dimensional velocity magnitude at (t=30 min.) and $Q=58$ l/s,

A-Circular Model, B-US-FRNP, C-DS-FRNP.

APPENDIX D

Figures of two-dimensional pressure distribution at different discharge.

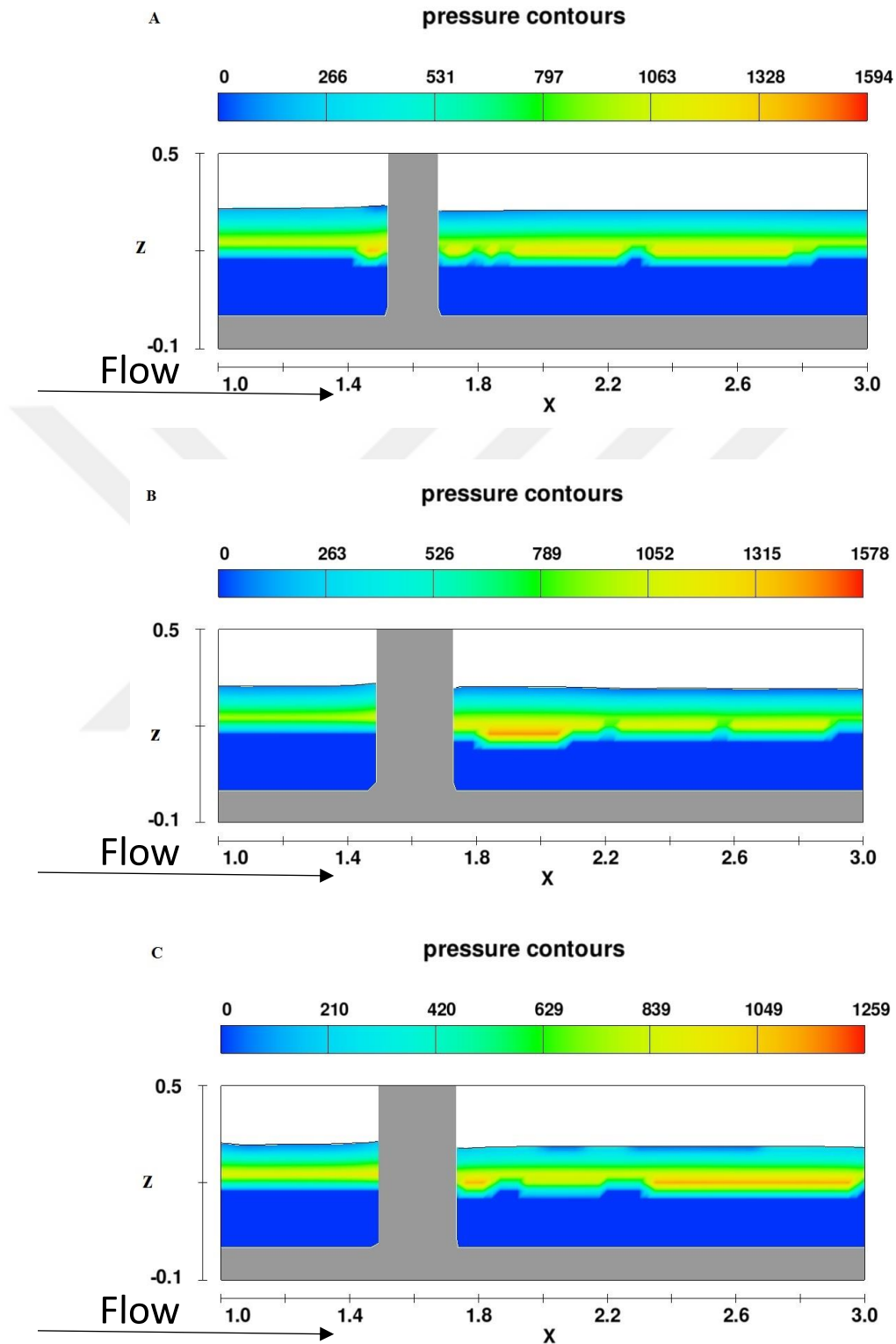


Figure D.1 Two-dimensional pressure distribution at (t=30 min.) and $Q=48$ l/s,

A-Circular Model, B-US-FRNP, C-DS-FRNP.

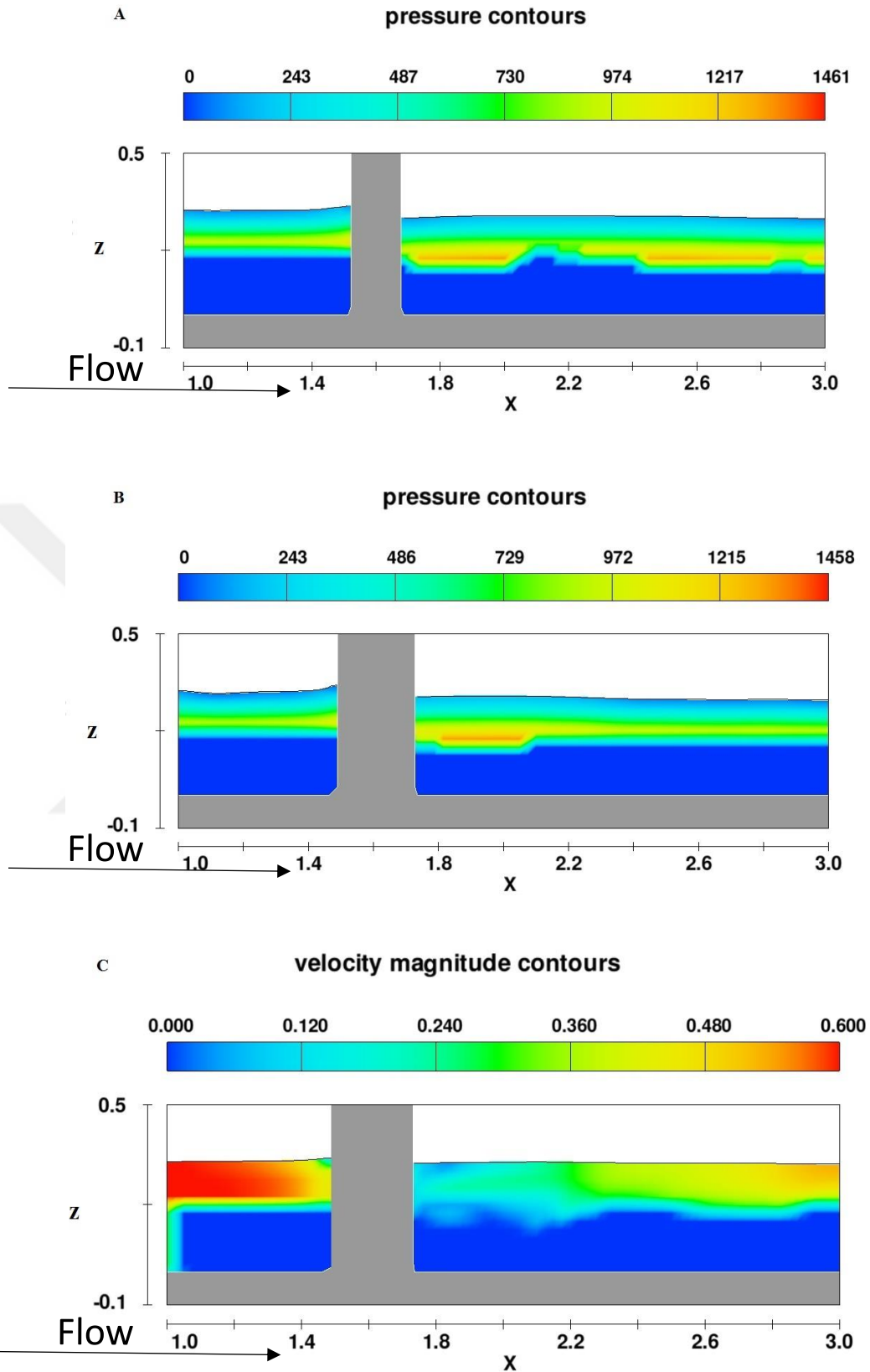


Figure D.2 Two-dimensional pressure distribution at (t=30 min.) and $Q=48$ l/s,

A-Circular Model, B-US-FRNP, C-DS-FRNP.